AD_____

Award Number: DAMD17-99-1-9120

TITLE: Comparative Structural Analysis of ERa and ERb Bound to Selective Estrogen Agonists and Antagonists

PRINCIPAL INVESTIGATOR: Geoffrey Greene, Ph.D.

CONTRACTING ORGANIZATION: The University of Chicago
Chicago, Illinois 60637

REPORT DATE: July 2000

TYPE OF REPORT: Annual

PREPARED FOR: U.S. Army Medical Research and Materiel Command
Fort Detrick, Maryland 21702-5012

REPORT DOCUMENTATION PAGE

Form Approved
OMB No. 074-0188

1. AGENCY USE ONLY (Leave blank)	2. REPORT DATE	3. REPORT TYPE AND DATES COVERED
	July 2000	Annual (14 Jun 99 - 13 Jun 00)

4. TITLE AND SUBTITLE
Comparative Structural Analysis of ERa and ERb Bound to Selective Estrogen Agonists and Antagonists

5. FUNDING NUMBERS
DAMD17-99-1-9120

6. AUTHOR(S)
Geoffrey Greene, Ph.D.

7. PERFORMING ORGANIZATION NAME(S) AND ADDRESS(ES)
The University of Chicago
Chicago, Illinois 60637

E-MAIL:
ggreene@ben-may

8. PERFORMING ORGANIZATION REPORT NUMBER

9. SPONSORING / MONITORING AGENCY NAME(S) AND ADDRESS(ES)
U.S. Army Medical Research and Materiel Command
Fort Detrick, Maryland 21702-5012

10. SPONSORING / MONITORING AGENCY REPORT NUMBER

11. SUPPLEMENTARY NOTES
Report contains color photos

12a. DISTRIBUTION / AVAILABILITY STATEMENT
Approved for public release; distribution unlimited

12b. DISTRIBUTION CODE

13. ABSTRACT *(Maximum 200 Words)*

The goal of this investigation is to determine the three-dimensional structures of the two known human estrogen receptors (ERα and ERβ) complexed with receptor-selective estrogens and antiestrogens (SERMs). The crystallographic structures of ERα and ERβ ligand binding domains complexed with *cis*-R,R-diethyl-tetrahydrochrysene-2,8-diol (R,R-THC) have been solved, suggesting mechanisms by which this compound can act as an ERα agonist and as an ERβ antagonist. Although agonists and antagonists bind at the same site within the core of the ER LBD, each induces distinct conformations in the transactivation domain (AF-2) of the LBD, especially in the positioning of helix 12, providing structural evidence for multiple mechanisms of selective agonism and antagonism. Previously determined structures of ERα with 4-hydroxytamoxifen (OHT) and diethylstilbestrol (DES) collectively revealed and defined a multipurpose docking site on ERα and ERβ that can accommodate either helix 12, in the presence of OHT, or one of several co-regulators in the presence of DES. Interestingly, R,R-THC antagonizes ERβ in a manner very different from OHT (and raloxifene), by filling the ligand binding pocket of ERβ sub-optimally and acting as a passive antagonist, a novel concept. In contrast, R,R-THC is clearly able to induce the agonist-bound conformation of helix 12 when bound to ERα, by making most of the same contacts as DES or estradiol. It is anticipated that the utilization structure based ligand design will allow the creation of new compounds that act differently on the two ERs and possess novel therapeutic properties that can be exploited to prevent or treat breast cancer.

14. SUBJECT TERMS
Breast CancerEstrogen receptors alpha and beta (ERα and ERβ); receptor structure; x-ray crystallography; selective estrogen receptor modulators (SERMs); agonism versus antagonism; hormone action

15. NUMBER OF PAGES
46

16. PRICE CODE

17. SECURITY CLASSIFICATION OF REPORT	18. SECURITY CLASSIFICATION OF THIS PAGE	19. SECURITY CLASSIFICATION OF ABSTRACT	20. LIMITATION OF ABSTRACT
Unclassified	Unclassified	Unclassified	Unlimited

NSN 7540-01-280-5500

Standard Form 298 (Rev. 2-89)
Prescribed by ANSI Std. Z39-18
298-102

FOREWORD

Opinions, interpretations, conclusions and recommendations are those of the author and are not necessarily endorsed by the U.S. Army.

___ Where copyrighted material is quoted, permission has been obtained to use such material.

___ Where material from documents designated for limited distribution is quoted, permission has been obtained to use the material.

X Citations of commercial organizations and trade names in this report do not constitute an official Department of Army endorsement or approval of the products or services of these organizations.

N/A In conducting research using animals, the investigator(s) adhered to the "Guide for the Care and Use of Laboratory Animals," prepared by the Committee on Care and use of Laboratory Animals of the Institute of Laboratory Resources, national Research Council (NIH Publication No. 86-23, Revised 1985).

X For the protection of human subjects, the investigator(s) adhered to policies of applicable Federal Law 45 CFR 46.

N/A In conducting research utilizing recombinant DNA technology, the investigator(s) adhered to current guidelines promulgated by the National Institutes of Health.

N/A In the conduct of research utilizing recombinant DNA, the investigator(s) adhered to the NIH Guidelines for Research Involving Recombinant DNA Molecules.

X In the conduct of research involving hazardous organisms, the investigator(s) adhered to the CDC-NIH Guide for Biosafety in Microbiological and Biomedical Laboratories.

Geoffrey Greene 7/28/00

ANNUAL REPORT FOR Award Number DAMD17-99-1-9120

TABLE OF CONTENTS

INTRODUCTION

Tamoxifen and raloxifene are effective in the treatment and prevention of hormone-dependent breast cancers while having beneficial effects on bone density and the cardiovascular system in women. These compounds are part of a growing class of structurally diverse molecules known as selective estrogen receptor modulators (SERMs), which can be distinguished from estrogens by their ability to act as either estrogen agonists or antagonists in different target tissues and hormonal environments. For example, while tamoxifen acts as a partial estrogen in the uterus and may increase the risk of uterine cancer, raloxifene acts as an antiestrogen in the uterus and may reduce the risk of uterine cancer. Both compounds appear to act as antiestrogens in the breast. The antiestrogenic and estrogenic effects of these compounds are mediated by one or both of two known estrogen receptors (ERα and ERβ). In view of the apparent concomitant as well as differential expression of ERα and ERβ in diverse estrogen target tissues, including the mammary gland, uterus, bone, brain, and vasculature, it is of great interest to identify and characterize compounds that can discriminate between, and selectively alter, the action of these receptors in such tissues. To add to this complexity, a recently described synthetic compound, R,R-5,11-*cis*-diethyl-5,6,11,12-tetrahydrochrysene-2,8-diol (R,R-THC), has been shown to act as a selective estrogen agonist when bound to ERα and as an antagonist when bound to ERβ.

An important, unresolved issue is the molecular mechanism(s) by which SERMs can act selectively as full agonists, partial agonists, or complete antagonists in the control of cell proliferation and cell fate in different tissues. To address this problem, we are using x-ray crystallography to determine the three-dimensional structures of the human ERα ligand binding domain (hERα-LBD) and the human ERβ ligand binding domain (hERβ-LBD) complexed with R,R-THC (ER subtype-selective estrogen/antiestrogen) as well as with other molecules that appear to act in like manner when complexed with either receptor. These include diethylstilbestrol (full agonist), 4-hydroxytamoxifen (mixed agonist/antagonist), ICI 182,780 (a complete antagonist) and GW5638 (mixed agonist/antagonist), a novel tamoxifen analog that functions in a manner that is distinct from other known ER modulators. Differences in each structure will be correlated with the molecular and cellular biology of ligand action via both receptors in several different cell and promoter contexts. We will also assess the ability of ERα and ERβ ligand complexes to interact with known coactivators and corepressors that participate in estrogen and antiestrogen action. In addition, a comparison of these structures with the previously determined structures of hERα-LBD bound to estradiol and raloxifene will provide valuable information about the structural/molecular differences that account for variable estrogen agonism and antagonism mediated by both ERα and ERβ. It is anticipated that structure information should help explain 1) how a single compound can act as an agonist when bound to ERα, and as an antagonist when bound to ERβ, and 2) how mixed antagonists, like tamoxifen and raloxifene, are able to elicit selective biological effects, via the same estrogen receptor, in different tissues such as the breast and uterus. The data thus obtained will have an impact both on our understanding of selective estrogen receptor modulators and on their design and use for the treatment and prevention of breast and uterine cancers.

Prior to the start of funding of this grant, we succeeded in determining the crystallographic structures of hERα LBD complexed with OHT and with DES. The latter complex included a peptide that represents the interaction domain of the p160 coactivator GRIP1/TIF2. These data were published (1) and a reprint is included in the Appendix. The following summary focuses on subsequent structural studies funded by this grant.

BODY

Background

Estrogens play a central role in mammalian physiology by regulating the differentiation, growth, and maintenance of a wide variety of tissues. For nearly thirty years, it was generally assumed that estrogens exerted their myriad effects by binding to and activating a single estrogen receptor (ER), the estrogen receptor α (ERα) (2, 3). This assumption was proven incorrect with the cloning and identification of a second estrogen receptor subtype, estrogen receptor β (ERβ) (4-6).

As might be expected, ERα and ERβ share many common structural and functional features. Both are members of the nuclear receptor (NR) superfamily of ligand-regulated transcription factors and exhibit the modular functional organization characteristic of most NRs: a central zinc finger DNA-binding domain (DBD) flanked by an amino-terminal domain and a carboxy-terminal ligand-binding domain (LBD). Although the sequences of the amino-terminal domains of ERα and ERβ share relatively little homology (~20% identity), the sequences of their DBDs and LBDs share 95% and 56% identity respectively (2, 3, 5). The sequence similarities in these two domains allow both ERs to bind the "classical" inverted hexanucleotide repeat estrogen response element (ERE) (7) and to bind many estrogens and antiestrogens with comparable affinities (8).

Each of the ER isoforms also possesses at least two functionally separable transcriptional activation functions (AFs), AF-1 within the amino-terminal domain and AF-2 within the LBD. The activity of the AF-1 of each ER is regulated by growth factor-inducible phosphorylation by MAP kinases (9, 10). In contrast, the activity of the AF-2 of each ER is stimulated by the binding of pure agonists, such as the endogenous estrogen 17β-estradiol (E2) and the synthetic stilbene estrogen diethylstilbestrol (DES), and blocked by the binding of pure antagonists, such as EM-800 and ICI-164,384 (11-14).

Despite these similarities, recent studies suggest that ERα and ERβ may play distinct roles in regulating gene expression *in vivo*. The two ERs have overlapping but distinct tissue distribution patterns; in rat, ERα is expressed in the uterus, testis, ovary, pituitary, kidney, epididymis, and adrenal glands and ERβ is expressed in the uterus, testis, ovary, prostate, lung, bladder, and brain (8). Consistent with these differences in localization, deletion of the ERα and ERβ genes in mice leads to substantially different phenotypes (15-17).

The two ERs may also play distinct roles in the mechanism of action of certain therapeutics. Selective estrogen receptor modulators (SERMs) such as tamoxifen and raloxifene (RAL) are currently being used to treat a wide variety of diseases including osteoporosis, cardiovascular disease, and breast cancer (18, 19). These compounds can function as either partial agonists or antagonists depending on the tissue and promoter context. Tamoxifen, for example, acts as an antagonist in mammary tissue but as a partial agonist in endometrial, skeletal, and cardiovascular tissues (20). In mammalian cells, ERα and ERβ appear to respond differently to SERMs. RAL and 4-hydroxytamoxifen (OHT) trigger different responses from ERα and ERβ at ER-dependent AP-1 enhancer elements (21). In addition, at classical EREs, OHT and RAL act as partial agonists on ERα but as pure antagonists on ERβ (11, 13). These functional differences coupled with the distinct expression patterns of the two ERs may result in the complex, tissue-specific effects of SERMs. Compounds which act by novel mechanisms on the two ERs might therefore be potentially novel SERMs. This hypothesis has engendered a great deal of interest in subtype-selective ER ligands.

In a recent search for ER subtype-selective ligands, the R,R enantiomer of 5,11-*cis*-diethyl-5,6,11,12-tetrahydrochrysene-2,8-diol (THC) was identified as a compound with a

modest preference for ERβ (K_d = 1.3 nM and 0.2 nM for full-length recombinant human ER_ and human ERβ respectively) (22, 23). In transfection experiments in human endometrial cancer (HEC-1) cells and other cell lines, THC acts as a full agonist on ERα but has little, if any, effect on the transcriptional activity of ERβ (22, 23). However, THC is able to very effectively antagonize the effect of E2 on ERβ in a dose-dependent manner (IC_{50} < 10 nM) (22, 23).

Given its activity profile, THC may act on ERα and ERβ by mechanisms distinct from those of OHT and RAL. The overall transcriptional activity of each ER results from the activities of both AF-1 and AF-2. For both ERα and ERβ, OHT and RAL act as AF-2 antagonists. The partial agonist character of these compounds on ERα in certain tissue and promoter contexts is thought to result from AF-1 activity (24). OHT and RAL are thought to act as pure ERβ antagonists because the transcriptional activity of ERβ is largely dominated by AF-2 (11, 13). THC is similar to OHT and RAL in that it acts as a pure ERβ antagonist. In contrast, THC functions as a full agonist on ERα. This suggests that either THC is able to induce a hyperactive state of AF-1 (while acting as an AF-2 antagonist) or it is able to elicit activity from both AF-1 and AF-2.

Recent structural studies indicate that NR ligands modulate AF-2 activity by differentially affecting the structure of NR LBDs (25). The binding of an AF-2 agonist to an NR LBD stabilizes a conformation of the LBD which favors the binding of transcriptional coactivators (26, 27). These coactivators, which enhance ligand-dependent transcription of NRs, are thought to serve as the bridge between agonist-bound LBDs and the general transcriptional machinery (28). Members of the p160 family of coactivators, including SRC-1/NCoA1 (29, 30), GRIP1/TIF2/NCoA2 (31-33), and p/CIP/RAC3/ACTR/AIB1 (33-36), recognize agonist-bound NR LBDs via short sequence motifs, LXXLL (where L is leucine and X is any amino acid) called NR boxes (33, 37-39). These NR boxes form amphipathic _-helices which recognize a hydrophobic groove on the surface of an agonist-bound LBD formed by residues from helices 3, 4, 5, and 12 (26, 27). In contrast, AF-2 antagonists such as OHT and RAL appear to stabilize an alternative conformation of the LBD that sterically precludes coactivator recognition (40, 41). Helix 12 in the antagonist-bound structures of the ERα and ERβ LBDs occludes the coactivator recognition groove by mimicking the interactions of the NR box with the LBD (40, 41). The recent structure of the ERβ LBD bound to the AF-2 partial agonist genistein (GEN) reveals that GEN binding drives helix 12 into yet a third conformation; helix 12 is bound over the ligand binding pocket in a position that only partially occludes the coactivator recognition surface (41). Depending on its actual mechanism of action, THC could induce either the agonist-bound, partial agonist-bound, or antagonist-bound conformations of the ERα LBD. However, given its effects on the transcriptional activity of ERβ, THC would be expected to induce the antagonist-bound conformation of the ERβ LBD.

To begin elucidating the mechanisms by which THC acts on the two ERs, we have used x-ray crystallography to determine the structure of the THC-ERα LBD-GRIP1 NR Box II peptide complex to 1.95 Å resolution and the structure of the THC-ERβ LBD complex to 2.85 Å resolution. The binding of THC to the ERα LBD stabilizes the agonist-bound conformation of helix 12. Remarkably, however, the binding of THC to the ERβ LBD stabilizes a conformation of helix 12 that most closely resembles that in the GEN-ERβ LBD complex (41). A comparison of these structures reveals the specific interactions that drive the differential positioning of helix 12 in the two complexes.

Results

Overall Structure of the THC-ERα LBD-GRIP1 NR Box II Peptide Complex

Although crystals of the THC-ERα LBD-GRIP1 NR Box II peptide complex and the DES-ERα LBD-GRIP1 NR Box II peptide complex were obtained under different conditions, the crystals of the two complexes lie in the same space group and have approximately the same cell dimensions (Experimental Procedures). Not surprisingly, the structures of the two complexes are virtually identical (0.45 Å root mean square deviation on all Cα atoms). The asymmetric unit of the THC complex crystals contains two LBDs arranged in the same dimeric configuration that has been observed in all previous structures of the ERα LBD (40, 42). Each LBD, a wedge-shaped molecule composed of a small beta hairpin and eleven to twelve helices arranged in three layers, is bound to a molecule of THC and a coactivator peptide (Figure 1A). Each THC molecule is completely enveloped within the lower subdomain of an LBD formed by residues from helices 3, 6, 7, 8, 11, and 12 and the S1/S2 hairpin (Figures 1A and 2A). Each coactivator peptide is bound in an α–helical conformation to a hydrophobic groove on the surface of an LBD formed by residues from helices 3, 4, 5, and 12 (Figure 1A).

THC Recognition by the ERα LBD

Overall, THC interacts with the ERα LBD in a manner analogous to the ways in which E2 and DES interact with the LBD (40, 42). The A ring of THC is bound in approximately the same position as the A rings of E2 and DES near helices 3 and 6. The A ring itself is recognized by the side chains of Ala 350, Leu 387, Leu 391, and Phe 404 and the A ring phenolic hydroxyl forms hydrogen bonds to the side chain carboxylate of Glu 353, to the guanidinium group of Arg 394, and to a buried water molecule (Figures 2A and 3). The A' ring of THC interacts with the opposite end of the binding pocket near helices 7, 8, and 11 which interacts with the D ring of E2 and the A' ring of DES. The A' ring forms van der Waals contacts with Met 421, Ile 424, Gly 521, and Leu 525 and the phenolic hydroxyl forms a hydrogen bond with the side chain imidazole of His 524 (Figures 2A and 4).

THC, E2, and DES, however, differ in their ability to fill the binding pocket. In the E2-LBD complex, there are unoccupied cavities adjacent to the α face of the B ring and the β face of the C ring of E2 (40, 42). DES is able to fill these cavities with its two ethyl groups. One of the ethyl groups of THC fills the cavity near the B ring by forming van der Waals contacts with Leu 391, Phe 404, Met 421, and Leu 428 (Figure 2A). The other ethyl group of THC points into the region of the binding pocket near the α face, instead of the β face, of the steroid C ring in the E2 complex. This ethyl group is, therefore, unable to fill the cavity near the C ring of E2 and instead forms van der Waals contacts with the side chains of both Leu 346 and Met 421 (Figure 2A). These packing interactions force the body of THC to be slightly angled (~10°) towards helix 12 relative to the body of E2.

Overall Structure of the THC-ERβ LBD Complex

The two ERβ LBD monomers in the THC-ERβ complex crystals do not interact to for the same dimer seen in the α complex. Instead, each of the two LBDs interact with symmetry-related molecules to form related but somewhat differently packed crystallographic trimers. The ERα LBD dimer has been shown to dissociate below pH 6.5, presumably through the protonation of one or more of the histidines at the dimer interface (43). Given that the residues involved in homodimerization are well conserved between the two isoforms (2, 3, 5), the high salt and low pH (~4.5) conditions used to obtain crystals of the THC-ERβ LBD complex should also favor the dissociation of the ERβ LBD dimer into monomers. These monomers presumably interact to form trimers either prior to or during the process of during crystal growth.

Despite these differences in quaternary structure, each of the two ERβ LBD monomers in the asymmetric unit adopts the same overall fold as the ERα LBD. As has been described previously (41), the ERβ LBD is also a wedge-shaped molecule formed from three layers of

eleven to twelve helices and a small beta hairpin (Figure 1B). The most notable feature of the conformation of the ERβ LBD bound to THC is that helix 12 is not positioned as it is in the ERα LBD-agonist complexes (40). Helix 12 is also not bound in the static region of the coactivator recognition groove as it is in the OHT- and RAL-ERα LBD complexes and the RAL-ERβ LBD complex (40, 41). Instead, helix 12 in the THC-ERβ LBD complex (Figures 1B and 5) interacts with the rest of the LBD in a manner most similar to that observed in the GEN-ERβ LBD complex (41).

The Conformation of Helix 12 in the THC-ERβ LBD Complex

Many of the same packing interactions dictate the positioning of helix 12 in both the THC (Figures 1B and 5) and the GEN-ERβ LBD complexes (41). As it does in the GEN complex, the side chain of Val 487, which forms van der Waals contacts with the side chains of Thr 299 and Leu 306, is inserted into the entrance of the ligand binding pocket formed by helices 3, 6, and 11 in the THC complex (Figure 5). The position of Val 487, which lies at the N-terminus of helix 12, forces the C-terminal end of helix 12 to project away from the body of the LBD (Figure 1B). As a result, the side chains of Leu 491, Met 494, and Leu 495, which mimic the interactions of the three NR box leucines with the static region of the coactivator recognition groove in the RAL-ERβ LBD complex (41), only partially occlude the coactivator binding site. The side chain of Leu 491, which lies almost directly above Val 487, packs against those of Leu 306, Glu 332, and Trp 335 (Figure 5). The side chain of Met 494 lies near helix 3 and packs against the side chains of Leu 306, Val 307, and Ile 310 (Figure 5). Leu 495 occupies approximately the same position as Leu 491 in the RAL-ERβ LBD complex (41) and packs against the side chains of Ile 310, Val 328, Leu 331, and Glu 332 (Figure 5). Overall, helix 12 in the THC and GEN-ERβ LBD complexes is tilted by ~25° relative to its orientation in the RAL-ERβ LBD complex (41). Although it is positioned similarly, the conformation of helix 12 in the THC complex is not identical to that in the GEN complex. Helix 12 is slightly shorter in the THC complex (residues 487 to 497) than helix 12 in the GEN complex (residues 487 to 499). In addition, whereas the side chain of Tyr 488 is well resolved in electron density maps of the GEN complex (41), it is not visible in maps of the THC complex. As a result, there is no evidence in the THC complex for the hydrogen bond between the phenolic hydroxyl of Tyr 488 and the side chain carboxylate of Glu 332 that is seen in the GEN complex.

THC Recognition by the ERβ LBD

THC is recognized in a similar but not identical manner by the ERβ LBD as it is by the ERα LBD. Although the two ethyl groups of THC are bound in similar locations, they are not in the same conformation in the two complexes. Whereas the two ethyl groups of THC are positioned underneath the body of the tetrahydrochrysene in the α complex, they are rotated outwards in the β complex (Figures 3 and 4). One of these ethyl groups forms nonpolar contacts with Leu 343 and Phe 356 (equivalent to Leu 391 and Phe 404 in ERα) and fills the unoccupied cavity near the α face of the B ring of E2 (Figure 2B). In order to accommodate the extended conformation of this moiety, the body of the tetrahydrochrysene is shifted outwards towards the entrance of the binding pocket near helices 3, 6, and 11 relative to its position in the α complex (Figures 3 and 4).

As a result of this positional shift, THC, in the β complex, is only able to form a subset of the interactions observed in the α complex (Figures 2A and 2B). As it is in the α complex, the phenolic A ring of THC, in the β complex, is recognized by the region of the binding pocket formed by residues from helices 3 and 6 and the beta hairpin. As described above, the A ring of THC forms van der Waals contacts with the side chains of four residues (Phe 404, Ala 350, Leu 387 and Leu 391) in the α complex. The A ring of THC, however, only interacts with the side

chains of three of the equivalent residues (Phe 356, Ala 302, and Leu 339) in the β complex (Figures 2A, 2B, and 3). The side chain of Leu 343 in ERβ (equivalent to Leu 391 in ERα) forms van der Waals contacts with one of the ethyl groups of THC instead of interacting with the A ring (Figure 2B). In the α complex, the side chains of Glu 353 and Arg 394 form van der Waals contacts with the A ring of THC, which presumably enhance the alignment of the hydrogen bonds formed between these residues and the phenolic A ring hydroxyl (Figures 2A and 3). Because it is bound somewhat more distantly from the equivalent residues (Glu 305 and Arg 346) in the β complex, THC does not form nonpolar contacts with the side chains of these residues and the A ring hydroxyl only forms a single hydrogen bond with the side chain carboxylate of Glu 305 (Figure 2B and 3).
In the β complex, the A' ring of THC is bound in the same region of the binding pocket as it is in the α complex and packs against Gly 472 and Leu 476 (equivalent to Gly 521 and Leu 525 in ERα) (Figures 2B and 4). However, the A' ring phenolic hydroxyl is positioned 0.9 Å distant from its position in the α complex and is, therefore, unable to form a hydrogen bond with the imidazole of His 475 as it does with His 524 in the α complex (Figure 4).

Discussion

The Binding of GEN and THC and Helix 12 Positioning

In mammalian cells, GEN and THC exhibit different activities on ERβ; GEN acts as a partial agonist and THC acts as a pure antagonist. And despite the fact that no residues from helix 12 appear to interact directly with either GEN (41) or THC (Figure 2B), helix 12 is in the same conformation in the GEN and THC-ERβ LBD complexes. How can this structural data be reconciled with the biological activity of these compounds?

The simplest model that is consistent with all of the existing structural and functional data begins with the hypothesis that, in the unliganded or apo-ERβ LBD, helix 12, adopts the same conformation as that observed in the GEN and THC complexes. The GEN/THC-bound conformation of helix 12 should prevent interaction with coactivator (and hence result in transcriptional inactivity of the LBD) for two reasons. First, the residues from helix 12 that are predicted to form part of the coactivator recognition or AF-2 surface are inappropriately positioned. Second, helix 12 itself is bound such that it partially occludes the static region of the AF-2 surface formed by residues from helices 3, 4, and 5. If the position of helix 12 in the apo-LBD is in the GEN/THC-bound conformation, this would be consistent with the observation that AF-2 is largely transcriptionally silent in the absence of ligand (11, 13). But in the absence of ligand, ER_ actually displays low but significant AF-2 mediated transcriptional activity (11). Hence, helix 12 in the apo-LBD must be in equilibrium between the GEN/THC-bound conformation and the agonist-bound conformation (as seen in the E2 and DES-ERα LBD complexes), which is properly aligned for coactivator recognition with the GEN/THC-bound conformation being heavily favored over the agonist-bound conformation (Figure 6).

The binding of ligands to the LBD would serve either to perturb or change the nature of this equilibrium. Agonist binding, by stabilizing the formation of interactions in and around the binding pocket , would promote AF-2 activity by shifting the equlibrium to favor the conformation of helix 12 that allows coactivator binding (Figure 6). The large basic side chains of OHT and RAL exit the binding pocket through the entrance formed by residues from helices 3, 6, and 11 and sterically preclude either the GEN/THC-bound or agonist-bound conformations of helix 12 which both involve helix 12 covering the entrance to the binding pocket (Figure 5) (41). In addition, antagonists like OHT and RAL induce structural distortions in and around the ligand binding pocket which disfavor the formation of interactions observed in agonist-bound structures of the LBD. In particular, these distortions cause helix 11 to be significantly shorter in

the antagonist complexes than in the agonist complexes. Therefore, the binding of these antagonists heavily favor a third and inactive conformation of the helix 12 in which helix 12 is bound to the static region of the coactivator binding groove, mimicking the interactions formed by an NR box with the rest of the LBD (Figure 6) (40, 41). This conformation of helix 12 makes the binding of coactivators to the OHT and RAL complexes even less favorable than binding to the apo-LBD and is consistent with the inverse agonism (or reduction in basal transcriptional activity) exhibited by these molecules in transcriptional assays (11).

Partial agonists, like GEN, would be ligands which are able to stabilize many, but not all, of the requisite interactions in and around the binding pocket that favor the agonist-bound or active conformation of helix 12. Although GEN appears to form many of the interactions with the ERβ ligand binding pocket that E2 and DES do with the ERα ligand binding pocket, helix 11 is shorter the GEN-ERβ LBD complex than in the agonist-bound ERα LBD complexes (41). Helix 11 in the GEN complex ends at His 475 as it does in the RAL-ERβ LBD complex (the length of helix 11 in the agonist-bound complexes precludes the GEN/THC-bound conformation as it does the OHT/RAL-bound conformation). So partial agonists, like GEN, may only partially shift the equilibrium in favor of the active conformation (Figure 6). In summary, the binding of coactivators to the GEN-ERβ LBD would be predicted to be much more favorable than binding to the OHT and RAL-LBD complexes, somewhat more favorable than binding to the apo-LBD, and less favorable than binding to the E2 or DES-LBD complexes. This would be consistent with the fact that the transcriptional activity of the GEN-bound ERβ is intermediate between that of pure-agonist bound ERβ and the apo-ERβ.

This model of partial agonist behavior is entirely consistent with structural and biological data on the peroxisome proliferator-activated receptor γ (PPARγ), the only nuclear receptor for which the apo and liganded structures of the LBD have been determined (27). In the apo-PPAR_ LBD structure, helix 12 is loosely bound to the LBD in a conformation that is inconsistent with coactivator recognition (27). When bound to the PPARγ LBD, PPAR_ agonists, such as rosiglitazone, form a series of indirect hydrogen bonds with the phenolic hydroxyl of Tyr 473 from helix 12 (27). This hydrogen bond network stabilizes a conformation of helix 12 that allows the binding of coactivators. The recent crystal structure of PPARγ with the weak partial agonist, GW0072, reveals that this ligand is able to fill the binding pocket without forming this hydrogen bond network. The conformation of helix 12 in this complex most closely resembles that in the apo-PPARγ LBD structure (44). The GW0072-PPARγ LBD complex is, however, able to interact with coactivators such as CBP and SRC-1 in mammalian two-hybrid experiments but to a much lesser extent than the rosiglitazone-PPAR_ LBD complex (44). This demonstrates that the binding of GW0072 does not preclude the active conformation of the PPARγ LBD, it simply does not favor this conformation as much as the binding of a full agonist. For PPARγ, then, partial agonists are simply molecules that can bind to the LBD but only partially shift the helix 12 conformational equilibrium to favor the agonist-bound conformation.

The limiting case of a partial agonist would be a ligand, which could form some interactions with the ligand binding pocket but could not stabilize enough of the appropriate interactions in and around the binding pocket to shift the conformational equilibrium of helix 12 towards the active conformation at all. As long as it were able to bind to the LBD with high affinity, this ligand could potentially antagonize the effects of agonists on the LBD. THC might well be such a ligand for the ERβ (Figure 6). THC acts like GEN in that it stabilizes a conformation of the LBD in which helix 11 ends at His 475. However, THC forms even fewer interactions with the ERβ LBD than GEN. Whereas, GEN forms hydrogen bonds with the side chains of Glu 305, Arg 346, and His 475 (41), THC is only able to form a single hydrogen bond with the γ–carboxylate of Glu 305. THC also forms fewer van der Waals contacts with the binding pocket than GEN (Figure 2B) (41).

The diffraction characteristics of the crystals of the THC complex also support the idea that THC interacts less optimally with the ERβ LBD than GEN. The relatively limited resolution of the data measured from these crystals (2.85 Å) largely results from the fact that the average intensity of the diffraction data falls off very rapidly as a function of resolution (Wilson B factor ~100 $Å^2$). By contrast, the crystals of the GEN complex do not suffer from the same problem and diffract to significantly higher resolution (1.8 Å) (41). In addition, diffraction images from the crystals of the THC complex show extensive evidence of thermal diffuse scatter. Both of these properties are suggestive that the molecules in the crystal lattice are undergoing large-scale breathing motions (45, 46). This would be expected if the LBD were not well packed around THC. The LBD, however, does appear to be well packed around GEN (41).

If the many interactions formed by GEN with the binding pocket are only able to partially shift the helix 12 equilibrium towards the agonist-bound conformation, then the even fewer interactions made by THC may not be able to influence the equilibrium at all. As a result, with respect to coactivator binding, the THC complex would be predicted to have a significantly lower affinity for coactivator than the GEN complex and perhaps one that was comparable to those of the OHT and RAL complexes. This would be consistent with the effects of THC on the transcriptional activity of ERβ.

THC Isoform Specific Interactions and "Antagonism Without Side Chains"

THC is clearly able to induce the agonist-bound conformation of helix 12 when it binds to the ERα LBD. A comparison of the ERα and ERβ complexes provides some clues as to the nature of the interactions that THC fails to form with the ERβ ligand binding pocket that result in its inability to shift the conformational equilibrium of helix 12 in ERβ. Of the approximately twenty-two residues which line the ligand binding pocket, there are only two residues which are not identical in the two ER isoforms: Leu 384 (ERα)/Met 336 (ERβ) and Met 421(ERα)/Ile 373(ERβ) (Figure 7). Given that neither Leu 384 nor Met 336 directly contact THC in their respective complexes, neither of these two residues would be expected to contribute substantially to the isoform specific interactions with THC (Figures 2A and 2B). By contrast, Met 421 in the ERα complex forms van der Waals contacts with the A' ring of and the two ethyl groups of THC, whereas Ile 373 in the ERβ complex does not interact at all with the ligand (Figures 2A and 2B). By forming the appropriate packing interactions, Met 421 aids in aligning the A' ring such that the phenolic hydroxyl forms a hydrogen bond with the imidazole side chain of His 524 (Figure 4). In addition, Met 421 and several other binding pocket residues, including Met 343, His 524, and Met 528, form a series of packing interactions between each other and the ligand. These cooperative packing interactions stabilize a length of helix 11 that favors the agonist-bound conformation of helix 12. In ERβ, the sidechain of Ile 373 is apparently either too small or not flexible enough to adopt the proper conformation necessary to interact with the ligand and Met 295, His 475, and Met 479 (equivalent to Met 343, His 524, and Met 528 in ERα). Hence, THC binding does not stabilize secondary structure to the same extent in ERβ as it does in ERα. Helix 11 as well as the two strands of the β-hairpin and helix 3 are shorter in the ERβ complex than they are in the ERα complex (Figure 8). The importance of Met 421 and Ile 373 to the isoform-specific effects of THC could be readily determined by analyzing the ligand binding and transcriptional properties of a mutant ERα in which Met 421 was mutated to an isoleucine and a mutant ERβ in which Ile 373 was mutated to a methionine.

In conclusion, the structures of THC bound to the LBDs of the two ERs reveals the mechanisms by which this compound acts. THC is a ERα AF-2 agonist and an ERβ AF-2 antagonist. THC antagonizes ERβ in a manner very different from OHT and RAL. OHT and RAL antagonize the receptor through side chain effects and the introduction of structural distortions in and around the binding pocket. In contrast, THC acts as a very weak partial

agonist by filling the ligand binding pocket of the ERβ LBD suboptimally. The utilization of subtype-specific interactions in ligand design should allow for creation of new compounds that act differently on the two ERs and possess novel therapeutic properties.

Experimental Procedures

Protein Expression and Purification

The human ERα LBD (residues 297-554) was expressed, carboxymethylated, and purified as previously described. The human ERβ LBD (residues 256-505) was expressed as a N-terminally hexahistidine-tagged fusion protein in BL21(DE3)pLysS harboring a derivative of pET-15b. Bacterial lysates were applied to an estradiol-Sepharose column and the bound ERβ LBD was carboxymethylated with 20 mM iodoacetic acid. Protein was eluted with 3 x 10^{-5} M THC in ~50 ml of 20 mM Tris·Cl, 1M Urea, and 10% DMF pH 8.1. The ERβ LBD was further purified by ion exchange chromatography (Resource Q, Pharmacia). Protein samples were analyzed by SDS-PAGE, native PAGE, and electrospray ionization mass spectrometry.

Crystallization and Data Collection

Crystals of the THC-ERα LBD-GRIP1 NR box II peptide complex were prepared by hanging drop vapor diffusion at 19-21°C . Prior to crystallization, the THC-ERα LBD complex was incubated overnight with a four-fold molar excess of the GRIP1 NR box II peptide. Samples (0.5 μL) of this solution (5.0 mg/mL protein) were mixed with 3.5 μL of reservoir buffer consisting of 16% (w/v) PEG 4000, 53 mM Tris·Cl (pH 8.8) and 50 mM $MgCl_2$ and suspended over wells containing 800 μL of the reservoir buffer. These crystals lie in the spacegroup $P2_1$ with cell dimensions a=54.55 Å, b=82.60 Å, c=59.04 Å and β=111.53°. Two molecules of the THC-LBD and two of the coactivator peptide form the asymmetric unit. A crystal was transferred to a cryosolvent solution containing 20% (w/v) PEG 4000, 15% (w/v) ethylene glycol, 100 mM Tris (pH 8.6), 100 mM $MgCl_2$ and frozen in an N_2 stream in a rayon loop. Diffraction data were measured at -170°C at beamline 5.0.2 at ALS using a ADSC Quantum 4 CCD camera at a wavelength of 1.10 Å. Images were processed with DENZO (47) and the integrated intensities were scaled with SCALEPACK (47) using the default -3σ cutoff.

Crystals of the THC-ERβ LBD complex were obtained by hanging drop vapor diffusion at 21-23°C. Samples (2 μL) of a solution of the complex (4.8 mg/mL) were combined with 2 μL samples of a reservoir solution containing 1.5-1.75 M $(NH_4)_2SO_4$ and 100 mM NaOAc pH 4.8-5.2 and suspended over wells containing 800 μL of reservoir solution. Crystals formed within 1-2 days. These crystals belong to the space group R3 with cell parameters a=b=99.14 Å and c=193.38 Å (hexagonal setting). The asymmetric unit contains two LBD monomers. Prior to data collection, a single crystal was transferred to a stabilizing solution (1.8 M $(NH_4)_2SO_4$, 100 mM NaCl, 100 mM NaOAc pH 4.5, and 10 μM THC). The crystal was then sequentially transferred at 30 minute intervals through a series of solutions consisting of the stabilizing solution supplemented with increasing concentrations of ethylene glycol (1% increments) to a final concentration of 15%. The crystal was then flash frozen in an N_2 stream in a rayon loop. Diffraction data were measured at -170°C at beamline 5.0.2 at ALS using a ADSC Quantum 4 CCD camera at a wavelength of 1.07 Å. Images were processed with DENZO and the integrated intensities were scaled with SCALEPACK using the default -3σ cutoff.

Structure Determination and Refinement

The side chains of Met 343, Leu 346, Glu 353, Leu 384, Leu 387, Met 388, Leu 391, Arg 394, Phe 404, Met 421, Ile 424, Leu 428, His 524, Leu 525, Met 528, and Leu 540 of both monomers were converted to alanine and the ligands, ions, carboxymethyl groups and waters were removed

from the DES complex model. The model was subject to rigid body refinement in REFMAC (48). The missing parts of the model were built and the rest of the model was corrected using MOLOC (49) and two-fold averaged maps generated in DM (50). All masks were generated using MAMA (51). Initially, positional refinement was carried out with REFMAC. At later stages, the model was refined using the simulated annealing, positional and B-factor refinement protocols in CNS (52) and a maximum-likelihood target. All B-factors were refined isotropically and anisotropic scaling and a bulk solvent correction were used. The R_{free} set contains a random sample of 6.5% of all data. In refinement, all data between 47 and 1.95 Å (with no σ cutoff) were used. The current model is composed of residues 305-460 and 469-547 of monomer A, residues 305-461 and 472-547 of monomer B, residues 687-697 of peptide A, residues 686-696 of peptide B, two ligand molecules, and two water molecules.

The intensities within the data set fall off very rapidly as a function of resolution (Wilson B factor ~100 $Å^2$ calculated from 4 to 2.85 Å). In order to increase the contribution of the higher resolution terms the data was sharpened with a correction factor of –50 $Å^2$. All subsequent manipulations were performed using this sharpened data.

The two LBDs in the asymmetric unit were located by molecular replacement in AMoRe (50) and TFFC (50). The search model was constructed by overlapping the models of five ERα LBD complexes (PDB Accession Numbers 1A52, 1ERE, 1ERR, 3ERD, and 3ERT) and setting the occupancies of each model to 0.2 (R= 55.3%, CC= 55.9% after placement of both monomers). The model was then rebuilt using MOLOC and two-fold averaged maps generated using DM (MAMA was used for all mask manipulations). Initially, refinement was carried out with using tight NCS restraints with REFMAC and later with the simulated annealing, positional and B-factor refinement protocols in CNS and a maximum-likelihood target. All B-factors were refined isotropically and anisotropic scaling and a bulk solvent correction were used. The R_{free} set contains a random sample of 5% of all data. In refinement, all data between 49 and 2.85 Å (with no σ cutoff) were used. The current model is composed of residues 259 to 501 of both monomers A and B, two ligand molecules, and two water molecules.

Illustrations

Figures 1, 3, 4, 5, and 8 were generated using BOBSCRIPT (53) and rendered using Raster3D (54). Figure 2 was generated using LIGPLOT (55).

KEY RESEARCH ACCOMPLISHMENTS

- Crystallographic structures of ERα LBD bound to 4-hydroxytamoxifen (OHT) and DES plus GRIP1 peptide solved (1) prior to start of funding of this grant.
- Crystallographic structures of ERα and ERβ LBDs bound to R,R-THC, an ERα agonist/ERβ antagonist, solved during year one.
- Molecular basis of estrogen agonism vs. antagonism predicted from structures of ERα and ERβ LBDs bound to estradiol, raloxifene, tamoxifen, DES, R,R-THC and TIF2/GRIP1 NR box II peptide.
- Positioning of helix 12 is a key discriminator between agonist- and antagonist-induced conformations of ERα and ERβ. A multipurpose docking site in the LBD can accommodate either coactivator (agonists) or helix 12 (antagonists).
- At least two mechanisms of ligand-induced antagonism: 1) side chain steric hindrance; 2) structural distortions in and around the ligand binding pocket.

- Molecular basis of ER subtype-selective agonism and antagonism predicted from structure of ERα and ERβ LBDs bound to R,R-THC.
- Novel concept of passive estrogen antagonism (antagonism without bulky side chains) predicted from R,R-THC-ERα/β structures.

REPORTABLE OUTCOMES

- Manuscripts, abstracts, presentations:
  Shiau et. al. (1) (see Appendix) published prior to funding. A second manuscript detailing the results reported here is in preparation and will be submitted for publication this year.
  Abstracts for several meetings included in Appendix.
  Presentation (no abstract): Symposium speaker; Hormones, Etiology, Prevention, and Treatment of Breast Cancer, Era of Hope Meeting, Department of Defense Breast Cancer Research Program, June 8-12, 2000, Atlanta, Georgia.

- patents: none
- degrees obtained with award support: none
- development of cell lines, etc: none
- informatics:
  R,R-THC-ERα/β crystallographic coordinates will be deposited in the PDB and will be released upon publication of the structures.
- funding applied for based on work supported by this award:
  I have applied for an R01 grant to complement, but not duplicate, the structural work represented by this DOD award, but no NIH funding has been awarded at this time.
- employment or research opportunities applied for: none

CONCLUSIONS

The goal of this investigation is to determine the three-dimensional structures of the two known human estrogen receptors (ERα and ERβ) complexed with receptor-selective estrogens and antiestrogens (SERMs). The crystallographic structures of ERα and ERβ ligand binding domains complexed with *cis*-R,R-diethyl-tetrahydrochrysene-2,8-diol (R,R-THC) have now been solved, suggesting mechanisms by which this compound can act as an ERα agonist and as an ERβ antagonist. Although agonists and antagonists bind at the same site within the core of the ER LBD, each induces distinct conformations in the transactivation domain (AF-2) of the LBD, especially in the positioning of helix 12, providing structural evidence for multiple mechanisms of selective agonism and antagonism. Previously determined structures of ERα with 4-hydroxytamoxifen (OHT) and diethylstilbestrol (DES) collectively revealed and defined a multipurpose docking site on ERα and ERβ that can accommodate either helix 12, in the presence of OHT, or one of several co-regulators in the presence of DES. Consistent with the prediction that bulky/extended side chains are not essential for antagonist behavior, R,R-THC antagonizes ERβ in a manner very different from OHT and RAL, by filling the ligand-binding pocket of ERβ sub-optimally and acting as a passive antagonist. Interestingly, while the R,R-THC-ERβ structure is similar to the published GEN-ERβ structure, the more extensive interactions of genistein with the residues that line the binding pocket of ERβ may partially shift the helix 12 equilibrium more toward the agonist-bound conformation, consistent with the partial agonism reported for genistein on ERβ. In contrast, when bound to ERα, R,R-THC is able to induce the agonist-bound conformation of helix 12 by making most of the same contacts as diethylstilbestrol (DES) or estradiol. It is anticipated that the utilization of subtype-specific

interactions in ligand design will allow the creation of new compounds that act differently on the two ERs and possess novel therapeutic properties. In addition, with the design and/or natural occurrence of compounds that selectively target ERα or ERβ, structure information should help reveal the molecular basis for such behavior.

So what? It is clear from the various solved structures for ERα and ERβ bound to diverse SERMs that the resulting ER conformations and ligand pharmacologies are not as simple as previously believed. Rather than just two distinct conformations of ER that reflect agonism or antagonism, it appears that multiple conformations are possible, each of which may mediate a different pharmacology for a particular ligand in a given tissue, such as the breast, uterus, bone, or cardiovascular system. Thus, it is important to solve a number of structures for both ERs complexed with ligands that have been shown to have different tissue-selective pharmacologies, such as GW5638 and ICI 182,780 (Faslodex). This type of information is essential both to understand as well as to design compounds that have ER subtype-selective and activity-selective behavior. A major goal of this investigation is to characterize and/or design compounds that are useful as chemopreventive agents, especially for breast and uterine cancers. To be useful in a clinical setting, such as hormone replacement therapy, such compounds must also have the beneficial effects of estrogen, including maintenance of bone density, protection of the cardiovasculature, prevention of hot flashes and perhaps delayed onset of Alzheimer's disease and maintenance of cognitive function. Whether or not it is possible to design a single molecule that can satisfy all of these requirements remains to be seen. However, it is clear that improved SERMs can be designed and/or discovered. Since most, if not all, of the behavior of the two known ERs is dictated by the conformations induced by diverse natural and synthetic ligands, determination of the corresponding 3D structures for representative SERMs should be a valuable tool for dissecting underlying molecular mechanisms and for designing new generation compounds. We will therefore continue in our efforts to determine and correlate ER-SERM structures with their biological activities.

REFERENCES

1. Shiau AK, Barstad D, Loria PM, Cheng L, Kushner PJ, Agard DA, Greene GL 1998 The structural basis of estrogen receptor/coactivator recognition and the antagonism of this interaction by tamoxifen. Cell 95:927-37
2. Green S, Walter P, Kumar V, Krust A, Bornert JM, Argos P, Chambon P 1986 Human oestrogen receptor cDNA: sequence, expression and homology to v- erb-A. Nature 320:134-9
3. Greene GL, Gilna P, Waterfield M, Baker A, Hort Y, Shine J 1986 Sequence and expression of human estrogen receptor complementary DNA. Science 231:1150-4
4. Kuiper G, Enmark E, Pelto-Huikko M, Nilsson S, Gustafsson J 1996 Cloning of a novel estrogen receptor expressed in rat prostate and ovary. Proc Natl Acad Sci 93:5925-5930
5. Mosselman S, Polman J, Dijkema R 1996 ER beta: identification and characterization of a novel human estrogen receptor. FEBS Lett 392:49-53
6. Tremblay GB, Tremblay A, Copeland NG, Gilbert DJ, Jenkins NA, Labrie F, Giguere V 1997 Cloning, chromosomal localization, and functional analysis of the murine estrogen receptor beta. Mol Endocrinol 11:353-65
7. Pace P, Taylor J, Suntharalingam S, Coombes RC, Ali S 1997 Human estrogen receptor beta binds DNA in a manner similar to and dimerizes with estrogen receptor alpha. J Biol Chem 272:25832-8
8. Kuiper GG, Carlsson B, Grandien K, Enmark E, Haggblad J, Nilsson S, Gustafsson JA 1997 Comparison of the ligand binding specificity and transcript tissue distribution of estrogen receptors alpha and beta. Endocrinology 138:863-70

9. Kato S, Endoh H, Masuhiro Y, Kitamoto T, Uchiyama S, Sasaki H, Masushige S, Gotoh Y, Nishida E, Kawashima H, Metzger D, Chambon P 1995 Activation of the estrogen receptor through phosphorylation by mitogen-actived protein kinase. Science 270:1491-1494
10. Tremblay A, Tremblay GB, Labrie F, Giguere V 1999 Ligand-independent recruitment of SRC-1 to estrogen receptor beta through phosphorylation of activation function AF-1. Mol Cell 3:513-9
11. Barkhem T, Carlsson B, Nilsson Y, Enmark E, Gustafsson J, Nilsson S 1998 Differential response of estrogen receptor alpha and estrogen receptor beta to partial estrogen agonists/antagonists. Mol Pharmacol 54:105-12
12. Kumar V, Green S, Stack G, Berry M, Jin J-R, Chambon P 1987 Functional domains of the human estrogen receptor. Cell 51:941-951
13. McInerney EM, Weis KE, Sun J, Mosselman S, Katzenellenbogen BS 1998 Transcription activation by the human estrogen receptor subtype beta (ER beta) studied with ER beta and ER alpha receptor chimeras. Endocrinology 139:4513-22
14. Tremblay A, Tremblay GB, Labrie C, Labrie F, Giguere V 1998 EM-800, a novel antiestrogen, acts as a pure antagonist of the transcriptional functions of estrogen receptors alpha and beta. Endocrinology 139:111-8
15. Couse JF, Korach KS 1999 Estrogen receptor null mice: what have we learned and where will they lead us? [published erratum appears in Endocr Rev 1999 Aug;20(4):459]. Endocr Rev 20:358-417
16. Ogawa S, Chan J, Chester AE, Gustafsson JA, Korach KS, Pfaff DW 1999 Survival of reproductive behaviors in estrogen receptor beta gene- deficient (betaERKO) male and female mice [In Process Citation]. Proc Natl Acad Sci U S A 96:12887-92
17. Windahl SH, Vidal O, Andersson G, Gustafsson JA, Ohlsson C 1999 Increased cortical bone mineral content but unchanged trabecular bone mineral density in female ERbeta(-/-) mice. J Clin Invest 104:895-901
18. Gradishar WJ, Jordan VC 1997 Clinical potential of new antiestrogens. J Clin Oncol 15:840-52
19. Jordan VC 1998 Antiestrogenic action of raloxifene and tamoxifen: today and tomorrow. J Natl Cancer Inst 90:967-71
20. Grese TA, Sluka JP, Bryant HU, Cullinan GJ, Glasebrook AL, Jones CD, Matsumoto K, Palkowitz AD, Sato M, Termine JD, Winter MA, Yang NN, Dodge JA 1997 Molecular determinants of tissue selectivity in estrogen receptor modulators. Proc Natl Acad Sci U S A 94:14105-10
21. Paech K, Webb P, Kuiper G, Nilsson S, Gustafsson J, Kushner P, Scanlan T 1997 Differential Ligand Activation of Estrogen Receptors ERα and ERβ at AP1 Sites. Science 277:1508-1510
22. Meyers MJ, Sun J, Carlson KE, Katzenellenbogen BS, Katzenellenbogen JA 1999 Estrogen receptor subtype-selective ligands: asymmetric synthesis and biological evaluation of cis- and trans-5,11-dialkyl- 5,6,11, 12- tetrahydrochrysenes. J Med Chem 42:2456-68
23. Sun J, Meyers MJ, Fink BE, Rajendran R, Katzenellenbogen JA, Katzenellenbogen BS 1999 Novel ligands that function as selective estrogens or antiestrogens for estrogen receptor-alpha or estrogen receptor-beta. Endocrinology 140:800-4
24. MacGregor JI, Jordan VC 1998 Basic guide to the mechanisms of antiestrogen action. Pharmacol Rev 50:151-96
25. Moras D, Gronemeyer H 1998 The nuclear receptor ligand-binding domain: structure and function. Curr Opin Cell Biol 10:384-91

26. Darimont BD, Wagner RL, Apriletti JW, Stallcup MR, Kushner PJ, Baxter JD, Fletterick RJ, Yamamoto KR 1998 Structure and specificity of nuclear receptor-coactivator interactions. Genes Dev 12:3343-56
27. Nolte RT, Wisely GB, Westin S, Cobb JE, Lambert MH, Kurokawa R, Rosenfeld MG, Willson TM, Glass CK, Milburn MV 1998 Ligand binding and co-activator assembly of the peroxisome proliferator-activated receptorγ. Nature 395:137-43
28. Glass CK, Rose DW, Rosenfeld MG 1997 Nuclear receptor coactivators. Curr Opin Cell Biol 9:222-32
29. Onate SA, Tsai SY, Tsai M-J, O'Malley BW 1995 Sequence and characterization of a coactivator for the steroid hormone receptor family. Science 270:1354-1357
30. Kamei Y, Xu L, Heinzel T, Torchia J, Kurokawa R, Gloss B, Lin SC, Heyman RA, Rose DW, Glass CK, Rosenfeld MG 1996 A CBP integrator complex mediates transcriptional activation and AP-1 inhibition by nuclear receptors. Cell 85:403-14
31. Hong H, Kohli K, Trivedi A, Johnson DL, Stallcup MR 1996 GRIP1, a novel mouse protein that serves as a transcriptional coactivator in yeast for the hormone binding domains of steroid receptors. Proc Natl Acad Sci USA 93:4948-4952
32. Voegel JJ, Heine MJS, Zechel C, Chambon P, Gronemeyer H 1996 TIF2, a 160 kDa transcriptional mediator for the ligand-dependent activation function AF-2 of nuclear receptors. EMBO J 15:3667-3675
33. Torchia J, Rose D, Inostroza J, Kamel Y, Westin S, Glass C, Rosenfeld M 1997 The transcriptional co-activator p/CIP binds CBP and mediates nuclear-receptor function. Nature 387:677-684
34. Anzick SL, Kononen J, Walker RL, Azorsa DO, Tanner MM, Guan X-Y, Sauter G, Kallioniemi O-P, Trent JM, Meltzer PS 1997 AIB1, a steroid receptor coactivator amplified in breast and ovarian cancer. Science 277:965-968
35. Chen H, Lin RJ, Schiltz RL, Chakravarti D, Nash A, Nagy L, Privalsky ML, Nakatani Y, Evans RM 1997 Nuclear receptor coactivator ACTR is a novel histone acetyltransferase and forms a multimeric activation complex with P/CAF and CBP/p300. Cell 90:569-80
36. Li H, Gomes PJ, Chen JD 1997 RAC3, a steroid/nuclear receptor-associated coactivator that is related to SRC-1 and TIF2. Proc Natl Acad Sci U S A 94:8479-84
37. Le Douarin B, Nielsen AL, Garnier JM, Ichinose H, Jeanmougin F, Losson R, Chambon P 1996 A possible involvement of TIF1 alpha and TIF1 beta in the epigenetic control of transcription by nuclear receptors. EMBO J 15:6701-15
38. Heery D, Kalkhoven E, Hoare S, Parker M 1997 A signature motif in transcriptional co-activators mediates binding to nuclear receptors. Nature 387:733-736
39. Ding S, Anderson C, Ma H, Hong H, Uht R, Kushner P, Stallcup M 1998 Nuclear receptor-binding sites of coactivators glucocorticoid receptor interacting protein 1 (GRIP1) and steroid receptor coactivator 1 (SRC-1): Multiple motifs with different binding specificities. Mol Endocrinol 12:302-313
40. Brzozowski A, Pike A, Dauter Z, Hubbard R, Bonn T, Engstrom O, Ohman L, Greene G, Gustafsson J, Carlquist M 1997 Molecular basis of agonism and antagonism in the oestrogen receptor. Nature 389:753-758
41. Pike AC, Brzozowski AM, Hubbard RE, Bonn T, Thorsell AG, Engstrom O, Ljunggren J, Gustafsson JA, Carlquist M 1999 Structure of the ligand-binding domain of oestrogen receptor beta in the presence of a partial agonist and a full antagonist. Embo J 18:4608-18
42. Tanenbaum DM, Wang Y, Williams SP, Sigler PB 1998 Crystallographic comparison of the estrogen and progesterone receptor's ligand binding domains. Proc Natl Acad Sci U S A 95:5998-6003

43. Thole HH 1994 The side chains responsible for the dimerization of the estradiol receptor by ionic bonds are lost in a 17 kDa fragment extending downstream from aa 303. J Steroid Biochem Mol Biol 48:463-6
44. Oberfield JL, Collins JL, Holmes CP, Goreham DM, Cooper JP, Cobb JE, Lenhard JM, Hull-Ryde EA, Mohr CP, Blanchard SG, Parks DJ, Moore LB, Lehmann JM, Plunket K, Miller AB, Milburn MV, Kliewer SA, Willson TM 1999 A peroxisome proliferator-activated receptor gamma ligand inhibits adipocyte differentiation. Proc Natl Acad Sci U S A 96:6102-6
45. Chang G, Spencer RH, Lee AT, Barclay MT, Rees DC 1998 Structure of the MscL homolog from Mycobacterium tuberculosis: a gated mechanosensitive ion channel. Science 282:2220-6
46. Clarage JB, Phillips Jr. GN 1997 Analysis of Diffuse Scattering and Relation to Molecular Motion. Methods Enzymol 277:407-432
47. Otwinowski Z, Minor W 1997 Processing of x-ray diffraction data collected in oscillation mode. Methods Enzymol 276:307-326
48. Murshudov GN, Vagin AA, Dodson EJ 1997 Refinement of macromolecular structures by the maximum-likelihood method. Acta Crystallogr D 53:240-255
49. Muller K, Amman HJ, Doran DM, Gerber PR, Gubernator K, Schrepfer G 1988 MOLOC: A molecular modeling program. Bull Soc Chim Belg 97:655-667
50. CCP4 1994 The CCP4 suite: programs for protein crystallography. Acta Crystallogr D 50:760-763
51. Kleywegt GJ, Jones TA, Halloween...masks and bones, in *From First Map to Final Model,* Bailey, S, *et al.*, Editors. 1994, SERC Daresbury Laboratory: Warrington, England.
52. Adams PD, Pannu NS, Read RJ, Brunger AT 1997 Cross-validated maximum likelihood enhances crystallographic simulated annealing refinement. Proc Natl Acad Sci U S A 94:5018-23
53. Esnouf RM 1997 An extensively modified version of MolScript that includes greatly enhanced coloring capabilities. J Mol Graph Model 15:132-4, 112-3
54. Merritt EA, Anderson WF 1994 Raster3D Version 2.0: A program for photorealistic molecular structures. Acta Crystallogr D 50:219-220
55. Wallace AC, Laskowski RA, Thornton JM 1995 LIGPLOT: a program to generate schematic diagrams of protein-ligand interactions. Protein Eng 8:127-34

FIGURE LEGENDS

Figure 1

A. Overall Structure of the THC-ERα LBD-GRIP1 NR Box II Peptide Complex. Two orthogonal views of the THC-ERα LBD-NR box II peptide complex. The coactivator peptide and the LBD are shown in ribbon representation. The peptide is colored gold and helix 12 is colored magenta. Helices 3, 4 and 5 are colored blue and THC, shown in space filling representation, is colored green.

B. Overall Structure of the THC-ERβ LBD Complex. Two orthogonal views of the THC-ERβ LBD complex similar to those of the ERα complex in **A**. The LBD is depicted in ribbon representation. Helix 12 is colored magenta and helices 3, 4 and 5 are colored blue. THC, in space filling representation, is colored red

Figure 2 THC Interactions with the ERα LBD (A.) and the ERβ LBD (B.). Residues that interact with THC are drawn at approximately their true positions. The residues that form van der Waals contacts with THC are depicted as labeled arcs with radial spokes that point towards the atoms of THC with which they interact. The residues that hydrogen bond to the ligand are shown in ball-and-stick representation. Hydrogen bonds are represented as dashed cyan lines; the distance of each bond is given. The ligand rings and the individual ligand atoms are labeled.

Figure 3 Interaction of the ERα LBD and the ERβ LBD with the A ring of THC. The structures of the ERα LBD and the ERβ LBD bound to THC were overlapped using the Cα coordinates of residues 306 to 526 from ERα and residues 259 to 476 from ERβ. The THC molecule bound to the ERα LBD is colored green and the THC molecule bound to the ERβ LBD is colored red. The ERα residue numbers are listed above the ERβ residue numbers. Hydrogen bonds are depicted as dashed orange bonds. In the THC-ERα LBD, the phenolic A ring of THC forms van der Waals contacts with the side chains of Ala 350, Leu 387, Leu 391, and Phe 404 and forms hydrogen bonds with the side chain carboxylate of Glu 353, the guanidinium group of Arg 394, and a buried water molecule. In the THC-ERβ LBD, the A ring of THC only packs against the side chains of Phe 356, Ala 302, and Leu 339 and forms a single hydrogen bond with the side chain of Glu 305.

Figure 4 Interaction of the ERα LBD and the ERβ LBD with the A' ring of THC. The structures of the two complexes were overlapped as in Figure 3. The THC molecule bound to the ERα LBD is colored green and the THC molecule bound to the ERβ LBD is colored red. The ERα and ERβ LBDs are colored gray and blue respectively. The ERα residue numbers are listed above the ERβ residue numbers. Hydrogen bonds are depicted as dashed orange bonds. In the THC-ERα LBD complex, the A' ring of THC forms van der Waals contacts with Met 421 and Ile 424 and the A' ring phenolic hydroxyl forms a hydrogen bond with the side chain imidazole of His 524. In the THC-ERβ complex, the A' ring of THC does not interact with any of the equivalent residues (Ile 373, Ile 376, and His 475).

Figure 5 The Helix 12/ERβ LBD Interface
A close-up view of the THC-ERβ LBD complex showing helix 12 bound to the static region of the coactivator binding site. Residues 481-501 are depicted a Cα worm and residues 487-497 colored magenta. The side chains of Val 487, Leu 491, Leu 494, and Leu 495 are shown. The side chains of only those LBD residues which interact with these residues from helix 12 are shown and are colored by atom type (carbon and sulfur atoms are colored green, oxygen atoms are colored red and nitrogen atoms are colored blue).

Figure 6 Ligands Perturb the Equilibrium Between Different Conformations of Helix 12. Schematic representations of the proposed conformational equilibria of the apo- and the various liganded states of the LBD are depicted. The three conformations of helix 12 (magenta), the GEN/THC-bound conformation, the OHT/RAL-bound conformation, and the E2/DES-bound conformation are labeled "Inactive I", "Inactive II", and "Active", respectively.

Figure 7 Alignment of the Sequences of the ERα LBD and the ERβ LBD. Identical residues in the sequences of the human ERα and ERβ LBDs are boxed. Residues which interact with the ligands are highlighted in green. The only residues that interact with THC which are different in the two ERs are Leu 384/Met 336 and Met 421/Ile 373.

Figure 8 THC Promotes Different Conformations of the ERα and ERβ LBDs. Ribbon representations of the THC-ERα LBD complex (without the coactivator peptide) and THC-ERβ LBD complex. In each complex, THC is shown in spacefilling representation and helix 12 is colored magenta. The regions of the two complexes which differ in secondary structural content are colored red.

A.

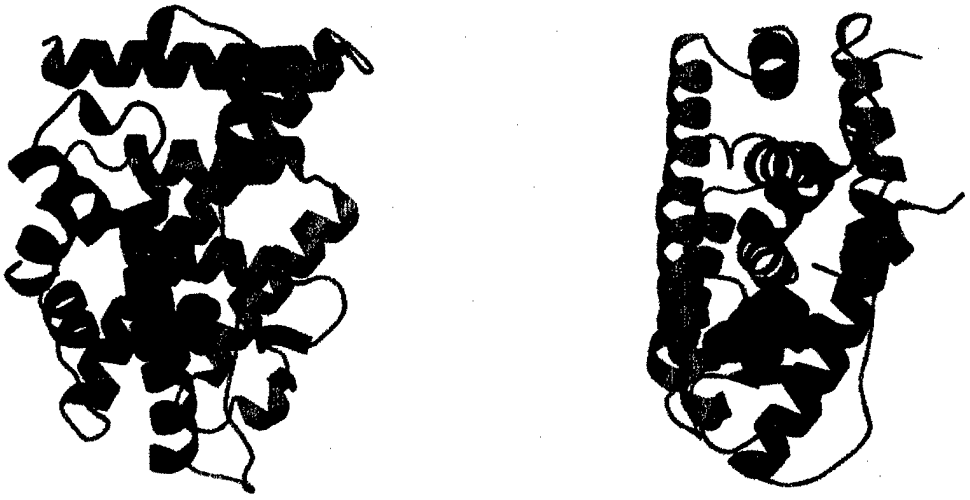

ERα

B.

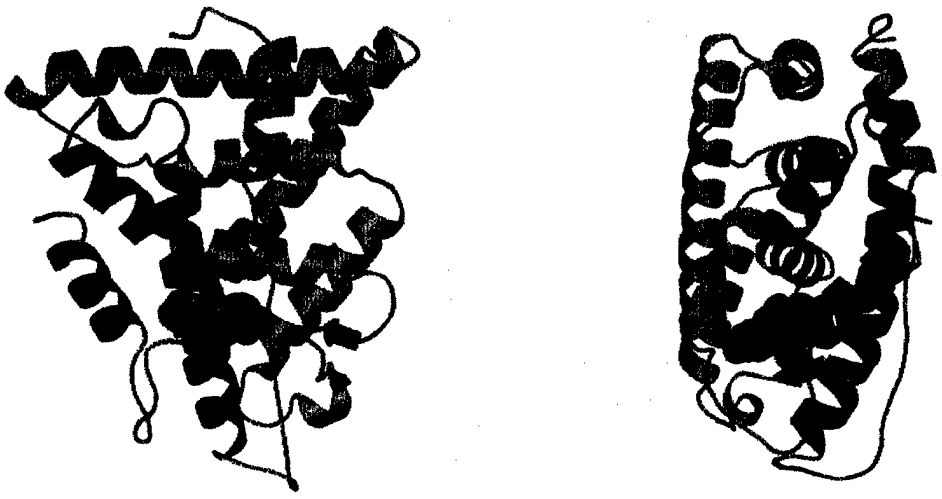

ERβ

Fig. 1

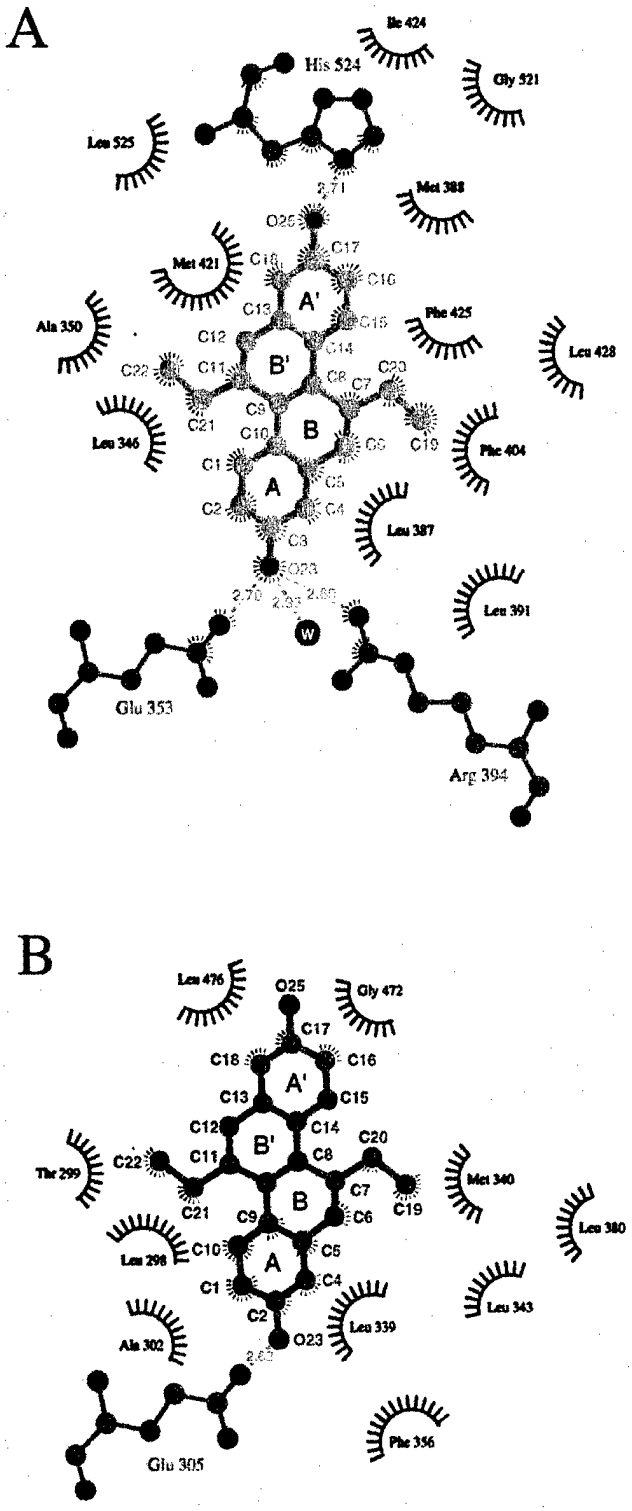
A
Ile 424
His 524
Gly 521
Leu 525
Met 388
Met 421
Ala 350
Phe 425
Leu 428
Leu 346
Phe 404
Leu 387
Leu 391
Glu 353
Arg 394
B
Leu 476
Gly 472
Thr 299
Met 340
Leu 380
Leu 298
Leu 343
Ala 302
Leu 339
Glu 305
Phe 356

Fig. 2

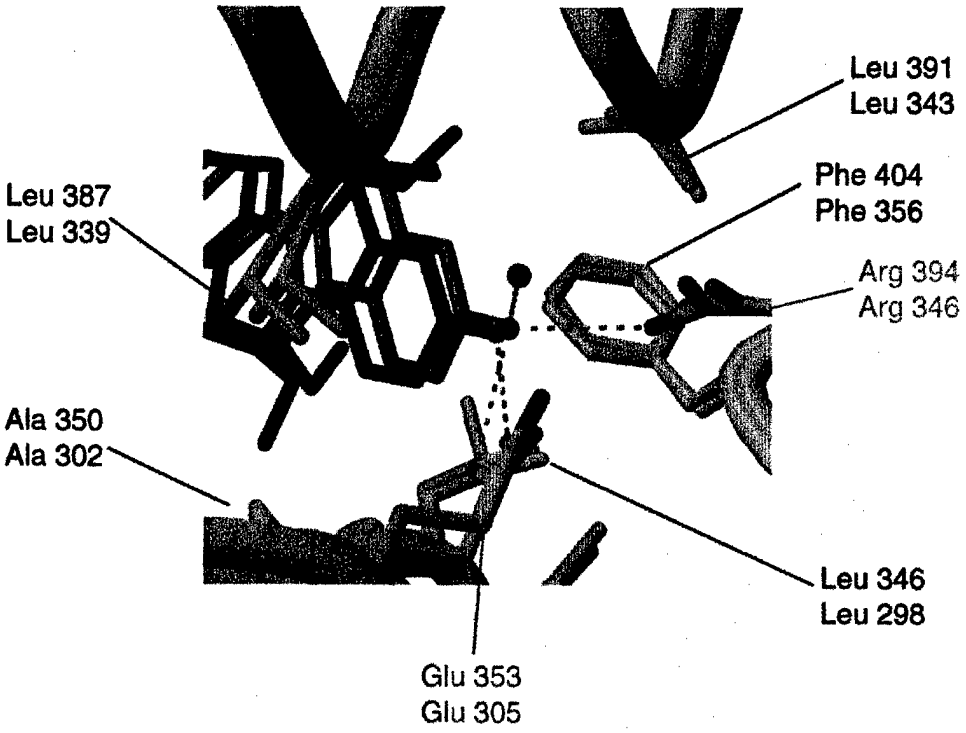
Leu 391
Leu 343
Phe 404
Phe 356
Leu 387
Leu 339
Arg 394
Arg 346
Ala 350
Ala 302
Leu 346
Leu 298
Glu 353
Glu 305

Fig. 3

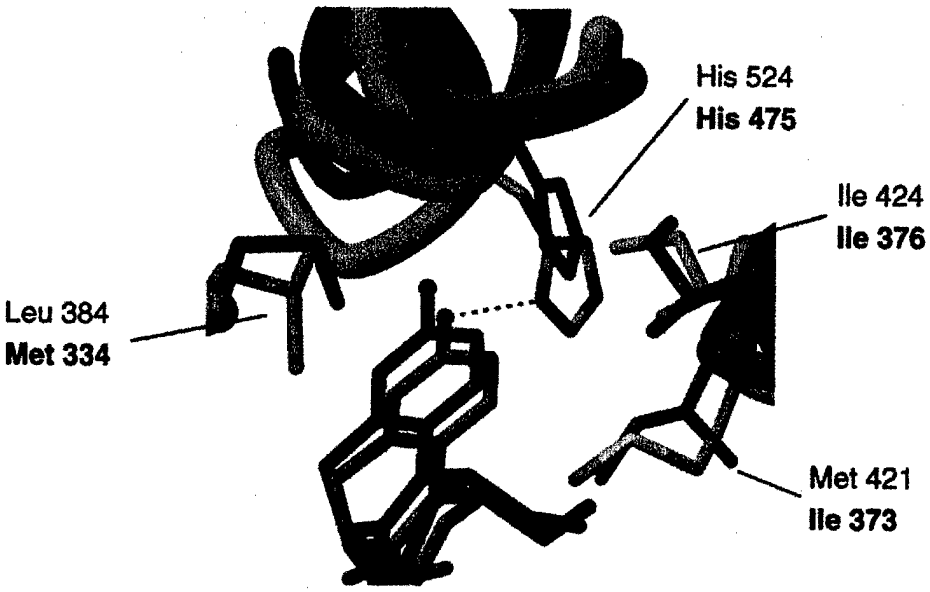

Fig. 4

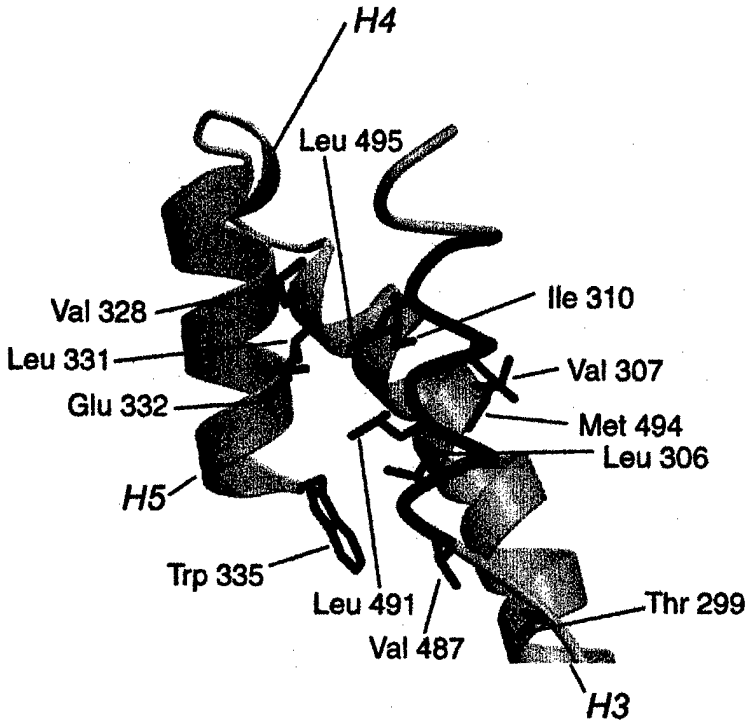
H4
Leu 495
Val 328
Leu 331
Glu 332
H5
Trp 335
Leu 491
Val 487
Ile 310
Val 307
Met 494
Leu 306
Thr 299
H3

Fig. 5

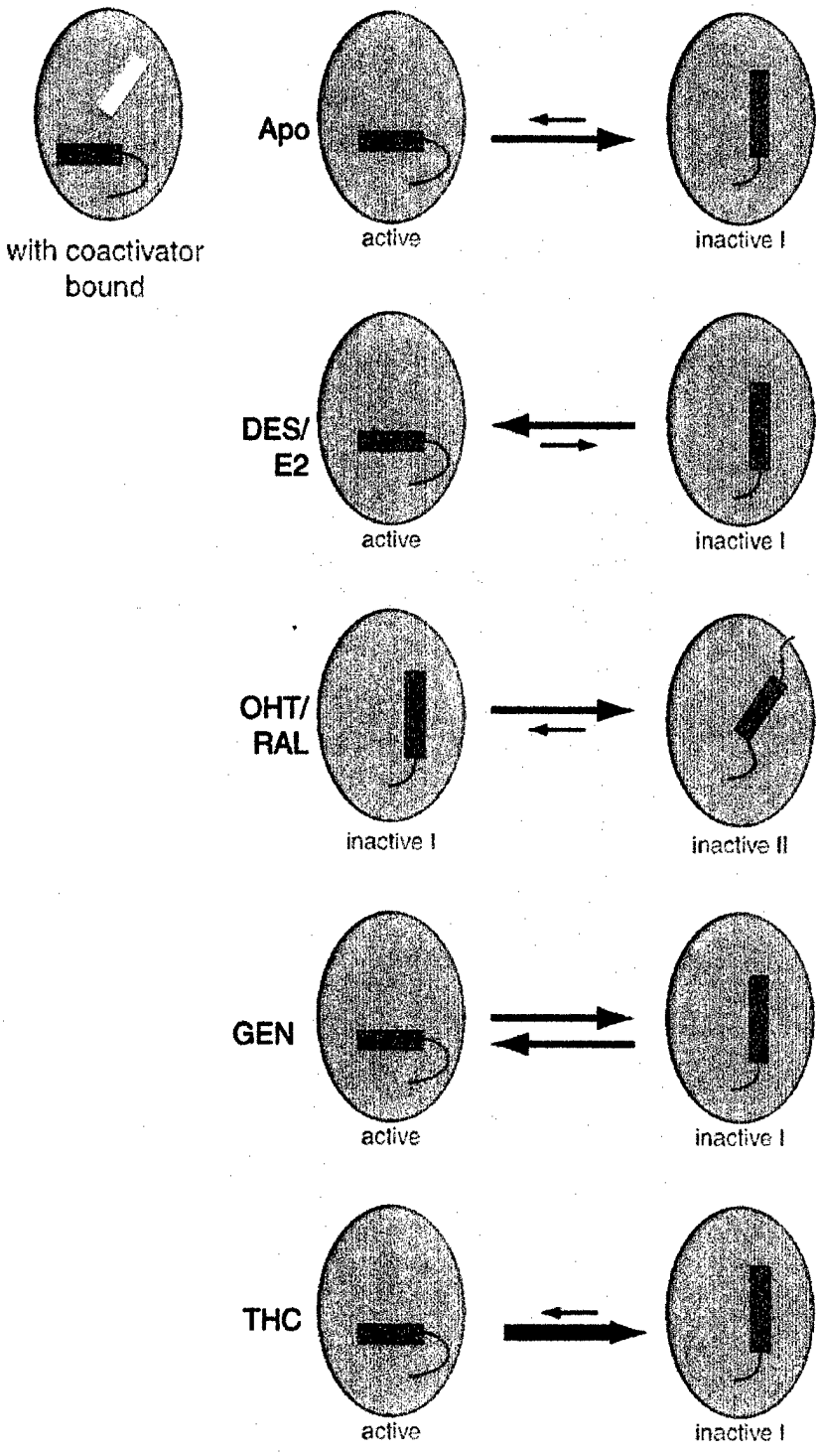
with coactivator bound
Apo
active
inactive I
DES/ E2
active
inactive I
OHT/ RAL
inactive I
inactive II
GEN
active
inactive I
THC
active
inactive I

Fig. 6

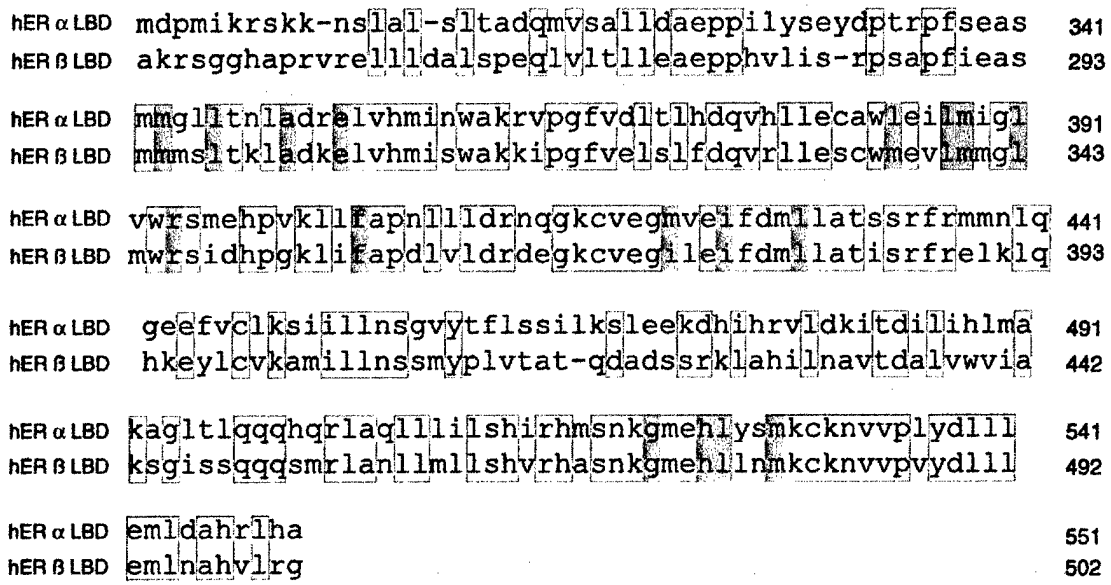
hERαLBD mdpmikrskk-nslal-sltadqmvsalldaeppilyseydptrpfseas 341
hERβLBD akrsgghaprvrelldalspeqlvltlleaepphvlis-rpsapfieas 293
hERαLBD mmgllinladrelvhminwakrvpgfvdltlhdqvhllecawleilmigl 391
hERβLBD mmmsltkladkelvhmiswakkipgfvelslfdqvrllescwmevlmmgl 343
hERαLBD vwrsmehpvkllfapnlldrnqgkcvegmveifdmllatssrfrmmnlq 441
hERβLBD mwrsidhpgkliiapdlvldrdegkcvegileifdmllatisrfrelklq 393
hERαLBD geefvclksiillnsgvytflssilksleekdhihrvldkitdiiihlma 491
hERβLBD hkeylcvkamillnssmyplvtat-qdadssrklahilnavtdalvwvia 442
hERαLBD kagltlqqqhqrlaqlllilshirhmsnkgmehlysmkcknvvplydlll 541
hERβLBD ksgissqqqsmrlanllmllshvrhasnkgmehllnmkcknvvpvydlll 492
hERαLBD emldahrlha 551
hERβLBD emlnahvlrg 502

Fig. 7

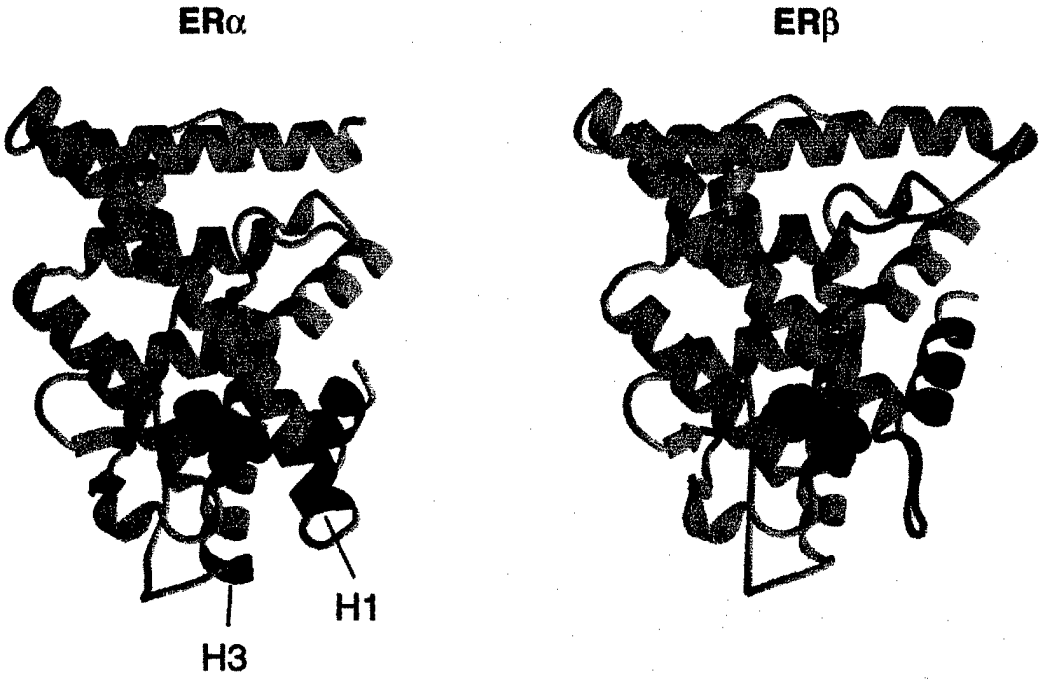

Fig. 8

ANNUAL REPORT FOR Award Number DAMD17-99-1-9120

APPENDIX

Journal article reprint:

1. Shiau AK, Barstad D, Loria PM, Cheng L, Kushner PJ, Agard DA, Greene GL 1998 The structural basis of estrogen receptor/coactivator recognition and the antagonism of this interaction by tamoxifen. Cell 95:927-37.

Selected abstracts of presentations at national or international meetings:

1. Breast Cancer, a Clinical Update, November 13, 1999, Huntington Beach, California.

2. Advances in Human Breast and Prostate Cancer, Keystone Symposia on Molecular and Cellular Biology, March 19-24, 2000, Incline Village, Nevada.

3. Eurocancer 2000, June 5-7, 2000, Paris, France.

Cell, Vol. 95, 927–937, December 23, 1998, Copyright ©1998 by Cell Press

The Structural Basis of Estrogen Receptor/Coactivator Recognition and the Antagonism of This Interaction by Tamoxifen

Andrew K. Shiau,* Danielle Barstad,† Paula M. Loria,† Lin Cheng,† Peter J. Kushner,‡ David A. Agard,*§ and Geoffrey L. Greene†§
*Howard Hughes Medical Institute
and the Department of Biochemistry and Biophysics
University of California at San Francisco
San Francisco, California 94143-0448
†The Ben May Institute for Cancer Research
and Department of Biochemistry and Molecular Biology
University of Chicago
Chicago, Illinois 60637
‡Metabolic Research Unit
University of California
San Francisco, California 94143

Summary

Ligand-dependent activation of transcription by nuclear receptors (NRs) is mediated by interactions with coactivators. Receptor agonists promote coactivator binding, and antagonists block coactivator binding. Here we report the crystal structure of the human estrogen receptor α (hERα) ligand-binding domain (LBD) bound to both the agonist diethylstilbestrol (DES) and a peptide derived from the NR box II region of the coactivator GRIP1 and the crystal structure of the hERα LBD bound to the selective antagonist 4-hydroxytamoxifen (OHT). In the DES-LBD-peptide complex, the peptide binds as a short α helix to a hydrophobic groove on the surface of the LBD. In the OHT-LBD complex, helix 12 occludes the coactivator recognition groove by mimicking the interactions of the NR box peptide with the LBD. These structures reveal the two distinct mechanisms by which structural features of OHT promote this "autoinhibitory" helix 12 conformation.

Introduction

Estrogens exert their physiological effects by binding to the estrogen receptors, which are members of the nuclear receptor (NR) superfamily of ligand-inducible transcription factors (Tsai and O'Malley, 1994; Beato et al., 1995). The estrogen receptor α (ERα) regulates the differentiation and maintenance of neural, skeletal, cardiovascular, and reproductive tissues (Korach, 1994; Smith et al., 1994). Compounds that modulate ERα transcriptional activity are currently being used to treat osteoporosis, cardiovascular disease, and breast cancer (Gradishar and Jordan, 1997; Jordan, 1998).

All ERα ligands bind exclusively to the C-terminal ligand-binding domain (LBD). The LBD recognizes a variety of compounds diverse in their size, shape, and chemical properties. Some of these ligands, including the endogenous estrogen 17β-estradiol (E_2) and the synthetic nonsteroidal estrogen diethylstilbestrol (DES), function as pure agonists, whereas others, such as ICI-164,384, function as pure antagonists. Synthetic ligands such as tamoxifen and raloxifene (RAL) belong to a growing class of molecules known as selective estrogen receptor modulators (SERMs), which function as antagonists in specific tissue and promoter contexts (Grese et al., 1997). The remarkable tissue-specific behavior of tamoxifen was recently demonstrated in the National Surgical Adjuvant Breast and Bowel Project–sponsored Breast Cancer Prevention Trial (Smigel, 1998). In the group of women at high risk for breast cancer who received tamoxifen treatment, there was an increased incidence of endometrial cancer but a reduced occurrence of certain bone fractures and a dramatic 45% reduction in breast cancer incidence. The rational design of new SERMs and the optimization of existing ones require an understanding of the effects of different ligand chemistries and structures upon ERα transcriptional activity.

Transcriptional activation by ERα is mediated by at least two separate activation functions (AFs), AF-1 in the N terminus, and AF-2 in the LBD. The activity of AF-1 is regulated by growth factors acting through the MAP kinase pathway (Kato et al., 1995), while AF-2 activity is responsive to ligand binding (Kumar et al., 1987). The binding of agonists triggers AF-2 activity, whereas the binding of antagonists does not (Berry et al., 1990).

Recent structural studies suggest that ligands regulate AF-2 activity by directly affecting the structure of the LBD. Comparison of the structure of the unliganded human retinoid X receptor α LBD (Bourguet et al., 1995) with the structures of the agonist-bound LBDs of the human retinoic acid receptor γ (RARγ) (Renaud et al., 1995) and other NRs suggests that an agonist-induced conformational change involving the repositioning of helix 12, the most C-terminal helix of the LBD, is essential for AF-2 activity (Moras and Gronemeyer, 1998). Because certain point mutations in helices 3, 5, and 12 abolish AF-2 activity but have no effect on ligand or DNA binding, these regions of the LBD have been predicted to form part of a recognition surface, created in the presence of agonist, for molecules that link the receptor to the general transcriptional machinery (Danielian et al., 1992; Wrenn and Katzenellenbogen, 1993; Henttu et al., 1997; Feng et al., 1998).

The structures of the LBD complexed with E_2 and RAL show that, although both ligands bind at the same site within the core of the LBD (Brzozowski et al., 1997), each of these ligands induces a different conformation of helix 12. Whereas helix 12 in the E_2-LBD complex packs against helices 3, 5/6, and 11 in a conformation that has been observed for the corresponding helix in other agonist-bound NR LBD structures, helix 12 in the RAL-LBD complex is bound in a hydrophobic groove composed of residues from helices 3 and 5. This alternative orientation of helix 12 partially buries residues in the groove that are necessary for AF-2 activity, suggesting that RAL and possibly other antagonists block AF-2 function by disrupting the topography of the AF-2 surface.

§To whom correspondence should be addressed (e-mail: agard@msg.ucsf.edu or ggreene@huggins.bsd.uchicago.edu).

Several proteins, including SRC-1/N-CoA1 (Onate et al., 1995; Kamei et al., 1996), GRIP1/TIF2/N-CoA2 (Hong et al., 1996; Voegel et al., 1996; Torchia et al., 1997;), p/CIP/RAC3/ACTR/AIB1 (Anzick et al., 1997; Chen et al., 1997; Li et al., 1997; Torchia et al., 1997), and CBP/p300 (Hanstein et al., 1996), associate in a ligand-dependent manner with the ERα. These proteins have been classified as transcriptional coactivators because they enhance ligand-dependent transcriptional activation by the ERα as well as by several other NRs (Horwitz et al., 1996; Glass et al., 1997). SRC-1 and GRIP1 bind to the agonist-bound LBDs of both the human thyroid receptor β (TRβ) and human ERα using the putative AF-2 interaction surface (Feng et al., 1998). Members of the p160 family of coactivators, such as SRC-1 and GRIP1, as well as other coactivators, recognize agonist-bound NR LBDs through a short signature sequence motif, LXXLL (where L is leucine and X is any amino acid), known as the NR box (Le Douarin et al., 1996; Heery et al., 1997; Torchia et al., 1997; Ding et al., 1998). Mutagenesis studies indicate that the affinity of coactivators for NR LBDs is determined principally, if not exclusively, by these NR boxes (Le Douarin et al., 1996; Heery et al., 1997; Torchia et al., 1997; Ding et al., 1998).

The structural mechanisms by which binding of different ligands to ERα influences coactivator recruitment remain unclear. We have chosen to examine the structural and functional effects on the LBD of the binding of two chemically related compounds, the agonist, DES, and the selective antagonist, 4-hydroxytamoxifen (OHT), the active metabolite of tamoxifen (Grainger and Metcalfe, 1996). Here we report the 2 Å resolution structure of the ERα LBD bound to both DES and a peptide with the sequence of the second NR box (NR box II) from the p160 coactivator GRIP1, and the 1.9 Å X-ray crystal structure of the human ERα LBD bound to OHT. In the DES complex, the NR box peptide is bound in an α-helical conformation by a hydrophobic groove formed by residues from helices 3, 4, 5, and 12 and the turn between helices 3 and 4. In the OHT complex, rather than forming part of a functional AF-2 surface, helix 12 binds to and occludes the coactivator recognition site by mimicking the interactions formed by an NR box with the LBD. The two distinct mechanisms by which specific structural features of OHT direct this alternative conformation of helix 12 are discussed.

Results

Structure Determination

GRIP1, a mouse p160 coactivator, interacts both in vivo and in vitro with the ERα LBD bound to agonist (Ding et al., 1998), but not with the LBD bound to antagonist (Norris et al., 1998). Mutational studies of GRIP1 and its human homolog TIF2 suggest that of the three NR boxes from GRIP1, NR box II (residues 690 to 694) binds most tightly to the ERα LBD (Ding et al., 1998; Voegel et al., 1998). Competition assays indicate that a 13-residue peptide, NH_2-KHKILHRLLQDSS-CO_2H (residues 686 to 698 from GRIP1), containing NR box II, binds specifically to the agonist-bound ERα LBD ($IC_{50} < 0.4$ μM; P. J. K., unpublished) and to other agonist-bound NR LBDs (Darimont et al., 1998 [see Note Added in Proof]; Ding et al., 1998). In the present study, an electrophoretic mobility shift assay was used to demonstrate that the NR box II peptide bound the ERα LBD in the presence of the agonist DES but not the antagonist OHT (data not shown). In combination, these observations suggest that the NR box II peptide is a valid model for studying the interaction between GRIP1 and the ERα LBD.

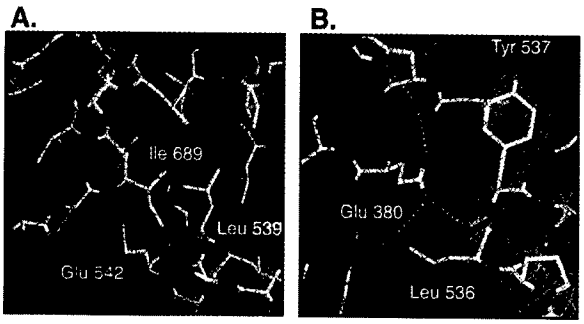

Figure 1. Views of the Electron Density of the DES-ERα LBD-GRIP1 NR Box II Peptide Complex and of the OHT-ERα LBD Complex

(A) A view of a $2F_o-F_c$ electron density map of the DES-LBD-peptide complex calculated at 2.03 Å resolution and contoured at 1.0 σ showing the GRIP1 NR box II interaction with the LBD. The peptide was omitted from the model prior to map calculation. Ile-689 from the peptide and two of the three receptor residues with which it interacts (Glu-542 and Leu-539) are labeled. Asp-538 has been omitted for clarity. The hydrogen bonds between the γ-carboxylate of Glu-542 and the amides of residues 689 and 690 of the peptide are depicted as dashed orange bonds.

(B) A view of a $2F_o-F_c$ electron density map of the OHT-LBD complex calculated at 1.90 Å resolution and contoured at 1.0 σ showing the N-terminal region of helix 12. The dashed orange bonds depict the water-mediated hydrogen bond network between the imidazole ring of His-377, the γ-carboxylate of Glu-380, and the amide of Tyr-537. The three labeled residues (Glu-380, Leu-536, and Tyr-537) interact with each other through van der Waals contacts and/or hydrogen bonds.

In order to characterize structurally the interaction between the GRIP1 NR box II peptide and the ERα LBD, recombinant human ERα LBD (residues 297–554) was crystallized bound to both DES and the peptide. The ERα LBD bound to OHT was also crystallized in order to determine the mechanism by which this antagonist blocks coactivator/ERα interaction. X-ray diffraction data from these crystals were measured, and the structures were determined by a combination of molecular replacement (using a modified version of the coordinates of the RARγ LBD [Renaud et al., 1995] as the search model) and aggressive density modification (see Experimental Procedures). The structure of the DES-ERα LBD-NR-box II peptide complex has been refined to a crystallographic R factor of 19.9% (R_{free} = 25.0%) using data to 2.03 Å resolution (Figure 1A and Table 1). The structure of the OHT-ERα LBD complex has been refined using data to 1.90 Å to a crystallographic R factor of 23.0% (R_{free} = 26.2%) (Figure 1B and Table 1).

Overall Structure of the DES-LBD-NR Box II Peptide Complex

The asymmetric unit of the DES-LBD-NR box II peptide complex crystals contains the same noncrystallographic dimer of LBDs that has been observed in the previously

Table 1. Summary of Crystallographic Statistics

Data Collection		
Ligand	DES	OHT
Space group	$P2_1$	$P6_522$
Resolution	2.03	1.90
Observations	104,189	269,253
Unique	30,265	23,064
Completeness (%)	98.4	99.1
R_{sym} (%)[a]	7.8	7.0
Average I/σI	9.8	16.1
Refinement		
No. of nonhydrogen atoms	4,180	2,069
R_{cryst} (%)[b]/R_{free} (%)	19.9/25.0	23.0/26.2
Bond rms deviation (Å)	0.005	0.006
Angle rms deviation (°)	1.05	1.04
Average B factor (Å²)	34.0	40.4

[a] $R_{sym} = \Sigma_i|I_i - \langle I_i\rangle|/\Sigma_i I_i$, where $\langle I_i\rangle$ is the average intensity over symmetry equivalents.
[b] $R_{cryst} = \Sigma|F_o - F_c|/\Sigma|F_o|$.

determined structures of the LBD bound to both E_2 and RAL (Brzozowski et al., 1997; Tanenbaum et al., 1998). The conformation of each LBD complexed with DES closely resembles that of the LBD bound to E_2 (Brzozowski et al., 1997); each monomer is a wedge-shaped molecule consisting of three layers of 11 to 12 helices and a single beta hairpin (Figure 2A). One NR box II peptide is bound to each LBD in a hydrophobic cleft composed of residues from helices 3, 4, 5, and 12 and the turn between 3 and 4 (Figures 2A and 3A). The density for both peptides in the asymmetric unit is continuous and unambiguous (Figure 1A). Residues 687 to 697 from peptide A and residues 686 to 696 from peptide B have been modeled; the remaining residues are disordered. Given that each peptide lies within a different environment within the crystal, it is striking that from residues Ile-689 to Gln-695 each peptide forms a two-turn, amphipathic α helix (Figures 2A and 3A). Flanking this region of common secondary structure, the peptides adopt dissimilar random coil conformations.

The NR Box II Peptide-LBD Interface

The binding of the NR box II peptide to the ERα LBD buries 1000 Å² of predominantly hydrophobic surface area from both molecules. The NR box II peptide-binding site is a shallow groove composed of residues Leu-354, Val-355, Ile-358, Ala-361, and Lys-362 from helix 3; Phe-367 and Val-368 from helix 4; Leu-372 from the turn between helices 3 and 4; Gln-375, Val-376, Leu-379, and Glu-380 from helix 5; and Asp-538, Leu-539, Glu-542, and Met-543 from helix 12 (Figure 3A). The floor and sides of this groove are completely nonpolar, but the ends of this groove are charged (Figure 3C).

The LBD interacts primarily with the hydrophobic face of the NR box II peptide α helix formed by the side chains of Ile-689 and the three LXXLL motif leucines (Leu-690, Leu-693, and Leu-694). The side chain of Leu-690 is deeply embedded within the groove and forms van der Waals contacts with the side chains of Ile-358, Val-376, Leu-379, Glu-380, and Met-543 (Figures 3A and 3C). The side chain of Leu-694 is similarly isolated within the groove and makes van der Waals contacts with the

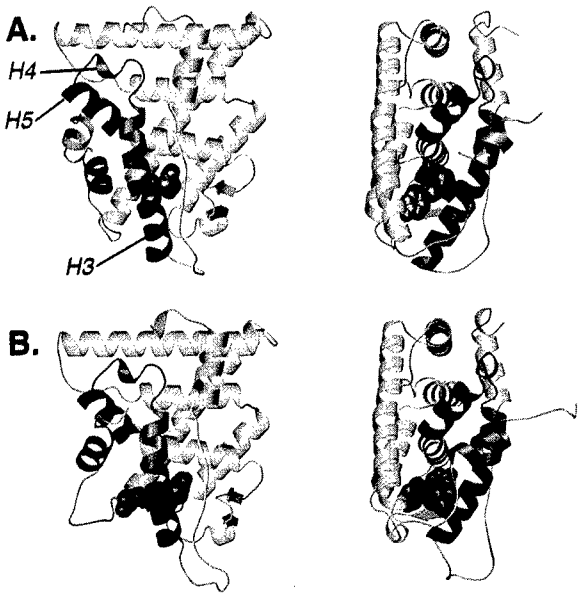

Figure 2. Overall Structures of the DES-ERα LBD-GRIP1 NR Box II Peptide Complex and of the OHT-ERα LBD Complex

(A) Two orthogonal views of the DES-ERα LBD-NR box II peptide complex. The coactivator peptide and the LBD are shown as ribbon drawings. The peptide is colored gold, and helix 12 (residues 538–546) is colored magenta. Helices 3, 4, and 5 (labeled H3, H4, and H5, respectively) are colored blue. DES, colored green, is shown in space-filling representation.

(B) Two orthogonal views of the OHT-ERα LBD complex similar to those of the agonist complex in (A). The LBD is depicted as a ribbon drawing. As in (A), helix 12 (residues 536–544) is colored in magenta, and helices 3, 4, and 5 are colored blue. OHT, in red, is shown in space-filling representation.

side chains of Ile-358, Lys-362, Leu-372, Gln-375, Val-376, and Leu-379 (Figures 3A and 3C). In contrast, the side chains of both Ile-689 and the second NR box leucine, Leu-693, rest against the rim of the groove (Figures 3A and 3C). The side chain of Ile-689 lies in a shallow depression formed by the side chains of Asp-538, Leu-539, and Glu-542. The side chain of Leu-693 makes nonpolar contacts with the side chains of Ile-358 and Leu-539.

In addition to interacting with the hydrophobic face of the peptide helix, the LBD stabilizes the main chain conformation of the NR box peptide by forming capping interactions with both ends of the peptide helix. Glu-542 and Lys-362 are positioned at opposite ends of the peptide-binding site (Figure 3A). The γ-carboxylate of Glu-542 hydrogen bonds to the amides of the residues of N-terminal turn of the peptide helix (residues 688 and 689 of peptide A; residues 689 and 690 of peptide B) (Figure 1A). Similarly, the ε-amino group of Lys-362 hydrogen bonds to the carbonyls of the residues of the C-terminal turn of the peptide helix (residue 693 of peptide A; residues 693 and 694 of peptide B) (Figure 5). The side chain of Gln-375 also forms a water-mediated hydrogen bond to the carbonyl of residue 694.

To test the importance of the NR box peptide/LBD interface observed in the crystal, a series of site-directed mutations were introduced into the LBD. These mutations were designed either to perturb the nonpolar character of the floor of the binding groove (Ile-358→Arg,

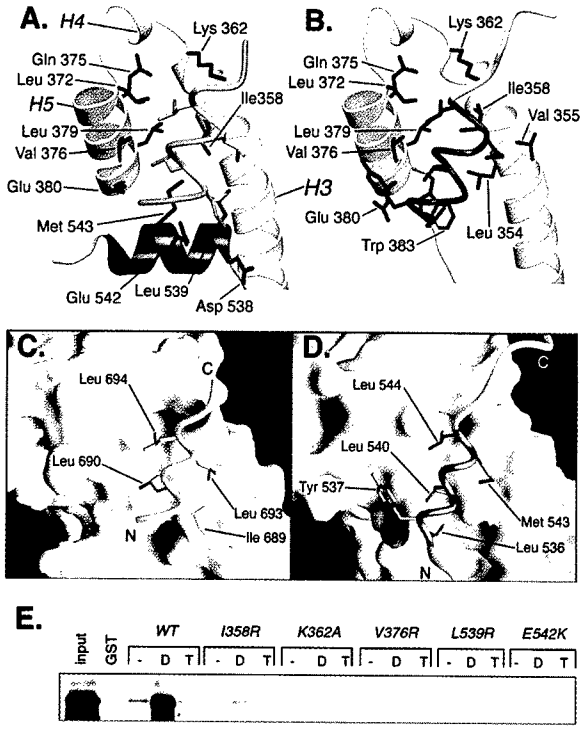

Figure 3. The NR Box II Peptide/DES-LBD Interface and the Helix 12/OHT-LBD Interface

(A) A close-up view of the coactivator peptide bound to the DES-LBD complex. The regions of the LBD that do not interact with the peptide have been omitted for clarity. Helices 3, 4, and 5 are labeled H3, H4, and H5, respectively. The side chains of the receptor residues that interact with the peptide are depicted. Except for Lys-362 (blue) and Glu-542 (red), the side chains are colored by atom type (carbon and sulfur atoms are colored green, oxygen atoms are colored red, and nitrogen atoms are colored blue). Helix 12 is colored magenta. The peptide, colored gold, is depicted as a Cα worm; only the side chains of Ile-689 and the three motif leucines (Leu-690, Leu-693, and Leu-694) are drawn.

(B) A close-up view of the OHT-LBD complex showing helix 12 bound to part of the coactivator-binding site. Only the side chains of residues that interact with helix 12 are drawn (with the exception of the side chain of His-373, which is omitted for clarity). Except for Lys-362 (blue) and Glu-380 (red), the side chains are colored by atom type (as specified in [A]). Residues 530–551 are depicted as a Cα worm; residues 536–544 are colored magenta. The side chains of Leu-536, Tyr-537, Leu-540, Met-543, and Leu-544 are shown.

(C) A molecular surface representation of the LBD bound to DES colored according to the local electrostatic potential (blue = positive; red = negative) as calculated in GRASP (Nicholls et al., 1991). The coactivator peptide is depicted as in (A) and the view is equivalent to that in (A). The side chains of Leu-690 and Leu-694 are bound in a hydrophobic groove, and those of Ile-689 and Leu-693 rest against the edge of this groove.

(D) A molecular surface representation of the LBD bound to OHT colored as in (C). Residues 530–551 are depicted as in (B) and the view is equivalent to that in (B). Whereas the side chains of Leu-540 and Leu-544 are embedded in the hydrophobic groove, that of Met-543 lies along the edge of this groove.

(E) ^{35}S-labeled GRIP1 was incubated with either immobilized glutathione S-transferase (GST), immobilized wild-type GST-hERα LBD (WT), or immobilized mutant GST-LBDs in the absence of ligand (–) or in the presence of DES (D) or OHT (T). Thirty picomoles of each of the GST-LBDs were immobilized, as described in the Experimental Procedures. The bound GRIP1 was visualized by fluorography after SDS-PAGE. The input lane represents the total amount of ^{35}S-GRIP1 included in each binding reaction. All of the mutations in the LBD disrupt agonist-dependent binding of GRIP1.

Val-376→Arg, and Leu-539→Arg) or to prevent the formation of the capping interactions (Lys-362→Ala and Glu-542→Lys) (Feng et al., 1998). Fusions of glutathione S-transferase (GST) to the wild-type and mutant LBDs were analyzed for their ability to bind ^{35}S-labeled GRIP1 in the absence of ligand or in the presence of DES or OHT. Only the wild-type GST-LBD was able to recognize the coactivator in the presence of DES (Figure 3E), confirming the importance of the observed capping and hydrophobic packing interactions.

Agonist Recognition

In its receptor complex, DES, like E_2 (Brzozowski et al., 1997), is completely encased within the narrower half of the LBD in a predominantly hydrophobic cavity composed of residues from helices 3, 6, 7, 8, 11, and 12 as well as the S1/S2 hairpin (Figures 2A and 4A).

The interaction of DES with ERα resembles that of E_2. One of the phenolic rings of DES lies in the same position as the E_2 A ring near helices 3 and 6. Like the aromatic ring of the E_2, the DES A ring (Figure 4A) is engaged by the side chains of Phe-404, Ala-350, Leu-387, and Leu-391 with its phenolic hydroxyl forming hydrogen bonds to the γ-carboxylate of Glu-353, to the guanidinium group of Arg-394, and to a structurally conserved water molecule. The A′ ring of DES (Figure 4A) is bound near helices 7, 8, and 11 adjacent to the location of the E_2 C and D rings. This ring forms van der Waals contacts not only with Gly-521 and Leu-525, like the D ring of E_2, but also with Met-343, Leu-346, and Met-421 (Figure 4A). Even though it is located 1.7 Å from the position of the D ring hydroxyl, the DES A′ ring phenolic hydroxyl is still able to hydrogen bond to the imidazole ring of His-524 (Figure 4A).

DES also forms contacts with the LBD that E_2 does not. There are unoccupied cavities adjacent to the α face of the B ring and the β face of the C ring of the E_2 (Brzozowski et al., 1997; Tanenbaum et al., 1998). The ethyl groups of DES, which project perpendicularly from the plane of the phenolic rings, fit snugly into these spaces. The resulting additional nonpolar contacts with the side chains of Ala-350, Leu-384, Phe-404, and Leu-428 (Figure 4A) may account for the higher affinity of DES for the receptor (Kuiper et al., 1997).

Except for Met-421 and Met-528 (both of which contact only DES) and Met-388 and Ile-424 (both of which contact only E_2), the ER is able to use the same residues to form all of the observed hydrogen bonds and van der Waals contacts with both of these distinctly shaped agonists (Figure 4A and Brzozowski et al., 1997; Tanenbaum et al., 1998). This remarkable adaptability is presumably the result of both the relatively large molecular volume of the binding pocket (~500 Å^3 in both complexes) and its apparent structural plasticity. In particular, at the DES A′ ring/steroid D ring end of the binding pocket, Met-343, Met-421, His-524, and Met-528 adopt different packing configurations in response to each ligand (data not shown).

Structure of the OHT-LBD Complex

The binding of OHT induces a conformation of the LBD that differs in both secondary and tertiary structural organization from that driven by DES binding. In the DES

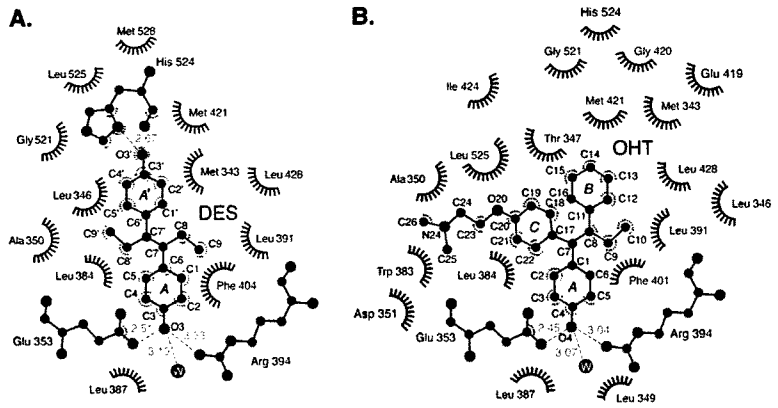

Figure 4. DES Interactions with the LBD (A) and OHT Interactions with the LBD (B)

Residues that interact with the ligands are drawn at approximately their true positions. The residues that form van der Waals contacts with ligand are depicted as labeled arcs with radial spokes that point towards the ligand atoms with which they interact. The residues that hydrogen bond to ligand are shown in ball-and-stick representation. Hydrogen bonds are represented as dashed cyan lines; the distance of each bond is given. The ligand rings and the individual ligand atoms are labeled.

complex, the main chain from residues 339 to 341, 421 to 423, and 527 to 530 forms parts of helices 3, 8, and 11, respectively. In contrast, these regions adopt an extended conformation in the OHT complex (Figures 2A, 2B, and 6A). In addition, the composition and orientation of helix 12 are different in the two structures. Helix 12 in the DES complex consists of residues 538 to 546, whereas helix 12 in the OHT complex consists of residues 536 to 544. Most dramatically, rather than covering the ligand-binding pocket as it does in the DES complex, helix 12 in the OHT complex occupies the part of the coactivator-binding groove formed by residues from helices 3, 4, and 5 and the turn connecting helices 3 and 4 (Figures 2A, 2B, and 3B). This alternative conformation of helix 12 appears to be similar to that observed in the RAL complex (Brzozowski et al., 1997).

Helix 12–LBD Interface

Except for the orientation of helix 12, the structure of the peptide-binding groove is almost identical in the DES-LBD-NR box II peptide, OHT-LBD, and E_2-LBD complexes (Figures 3A and 3B) (Brzozowski et al., 1997). We therefore refer to the region of this groove outside of helix 12 as the "static region" of the NR box–binding site (Feng et al., 1998). Helix 12 in the OHT complex and the NR box peptide helix in the DES complex interact with the static region of the coactivator recognition groove in strikingly similar ways.

Helix 12 mimics the hydrophobic interactions of the NR box peptide with the static region of the groove with a stretch of residues (residues 540 to 544) that resembles an NR box (LLEML instead of LXXLL). The side chains of Leu-540 and Met-543 lie in approximately the same locations as those of the first and second motif leucines (Leu-690 and Leu-693) in the peptide complex (Figure 5). Leu-540 is inserted into the groove and makes van der Waals contacts with Leu-354, Val-376, and Glu-380 (Figures 3B and 3D). Met-543 lies along the edge of the groove and forms van der Waals contacts with the side chains of Leu-354, Val-355, and Ile-358 (Figures 3B and 3D). The side chain position of Leu-544 almost exactly overlaps that of the third NR box leucine, Leu-694 (Figure 5). Deep within the groove, the Leu-544 side chain makes van der Waals contacts with the side chains of Ile-358, Lys-362, Leu-372, Gln-375, Val-376, and Leu-379 (Figures 3B and 3D).

Helix 12 in the OHT complex is also stabilized by N- and C-terminal capping interactions. Lys-362 interacts with the C-terminal turn of helix 12 much as it does with the equivalent turn of the peptide helix (Figures 3A and 3B). The Lys-362 side chain packs against the C-terminal turn of helix 12 with its ε-amino group hydrogen bonding to the carbonyls of residues 543 and 544 (Figure 5). Given that the capping interaction at the N-terminal turn of the coactivator helix is formed by a helix 12 residue (Glu-542), the N-terminal turn of helix 12 in the antagonist complex is stabilized by another residue, Glu-380 (Figures 3B and 3D). The Glu-380 γ-carboxylate forms van der Waals contacts with Tyr-537 and interacts with the amide of Tyr-537 through a series of water-mediated hydrogen bonds (Figure 1B).

In addition to forming these "NR box–like" interactions, helix 12 also forms van der Waals contacts with areas of the LBD outside of the coactivator recognition groove. The side chain of Leu-536 forms van der Waals contacts with Glu-380 and Trp-383, and that of Tyr-537 forms van der Waals contacts with His-373, Val-376,

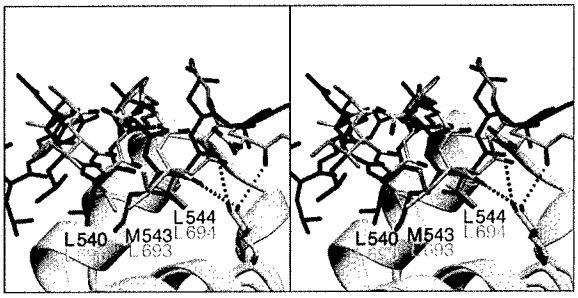

Figure 5. Comparison of Helix 12 from the OHT Complex and the NR Box II Peptide

The structures of the OHT-LBD complex and the DES-LBD-NR box II peptide complex were overlapped using the Cα coordinates of residues 306–526 of the LBD. Helix 12 from the DES-LBD-coactivator peptide complex is omitted for clarity. Residues 536–551 (helix 12 = residues 536–544) from the OHT-LBD complex are colored magenta, and the peptide is colored gold. For the OHT-LBD complex, the hydrogen bonds between the ε-amino group of Lys-362 and the backbone carbonyls of residues 543 and 544 of helix 12 are illustrated as dashed magenta bonds. For the DES-LBD-peptide complex, the hydrogen bonds between the ε-amino group of Lys-362 and the backbone carbonyls of residues 693 and 696 of the coactivator peptide are depicted as dashed orange bonds. Helix 12: L540 = Leu-540; M543 = Met-543; L544 = Leu-544. Peptide: L690 = Leu-690; L693 = Leu-693; L694 = Leu-694.

and Glu-380 (Figures 1B, 3B, and 3D). As a result of these contacts, helix 12 in the OHT complex buries more solvent-accessible surface area (~1200 Å^2) than the NR box peptide in the DES complex.

OHT Recognition

OHT is bound within the same pocket that recognizes DES, E_2, and RAL. The orientation of OHT within the binding pocket appears to be dictated by the positioning of two structural features of this ligand, the phenolic A ring and the bulky side chain (Figures 4B and 6C). The A ring of OHT is bound in approximately the same location as the A ring of DES near helices 3 and 6, with its phenolic hydroxyl hydrogen bonding to a structurally conserved water and to the side chains of Glu-353 and Arg-394 (Figure 4B). Like the bulky side chain of RAL, the side chain of OHT exits the binding pocket between helices 3 and 11 (Figures 2B and 4B). The OHT C ring (Figure 4B) forms van der Waals contacts with the side chains of Met-343, Leu-346, Thr-347, Ala-350, Trp-383, Leu-384, Leu-387, and Leu-525. The positioning of the flexible dimethylaminoethyl region of the side chain is stabilized by van der Waals contacts with Thr-347, Ala-350, and Trp-383 and by a salt bridge between the dimethylamino group of the side chain and the β-carboxylate of Asp-351, which lies 3.8 Å away (Figure 4B). The positions of the A ring and the side chain in the context of the rigid triphenylethylene framework of OHT requires that the ethylene group of OHT lie in an orientation nearly orthogonal to that of the ethylene group of DES (Figures 4A, 4B, and 6D). As a result, the B ring of OHT is driven more deeply into the binding pocket than the A′ ring of DES (Figures 6B and 6C).

This location of the OHT B ring apparently cannot be accommodated by the same mechanisms that allow the DES A′ ring/E_2 D ring end of the binding pocket to adapt to the different structural features of DES and E_2. Instead, the residues that contact the B ring (Met-343, Leu-346, Met-421, Ile-424, Gly-521, His-524, and Leu-525), most of which also interact with the A′ ring of DES, adopt conformations distinct from the ones they adopt in the DES structure (Figure 6D). In fact, the location of the B ring actually precludes the side chain of one residue, Met-421, from adopting the same conformation that it adopts in the DES structure (Figures 6B and 6C). As a consequence of these B ring–induced side chain conformations, many interresidue van der Waals contacts present in the DES complex are absent in the OHT complex. For example, whereas Met-421 packs against His-524 from helix 11 and against Met-343 from helix 3 in the agonist complexes, it is precluded by the location of the OHT B ring from interacting with either of these residues in the antagonist complex (Figure 6D).

The structural effects of the placement of the B ring are not limited to the residues that contact the B ring; the conformations of these residues force other residues throughout the binding pocket to, in turn, adopt alternative conformations. For instance, the conformation of Met-421 in the OHT complex prevents the side chains of Phe-404 and Phe-425 from occupying the positions they take in the DES complex (Figures 6B and 6C). The alternative conformations of the side chains of both the residues that directly contact the B ring and those that are indirectly affected by it force the main chain throughout the binding pocket to adopt a different conformation as well (Figure 6D).

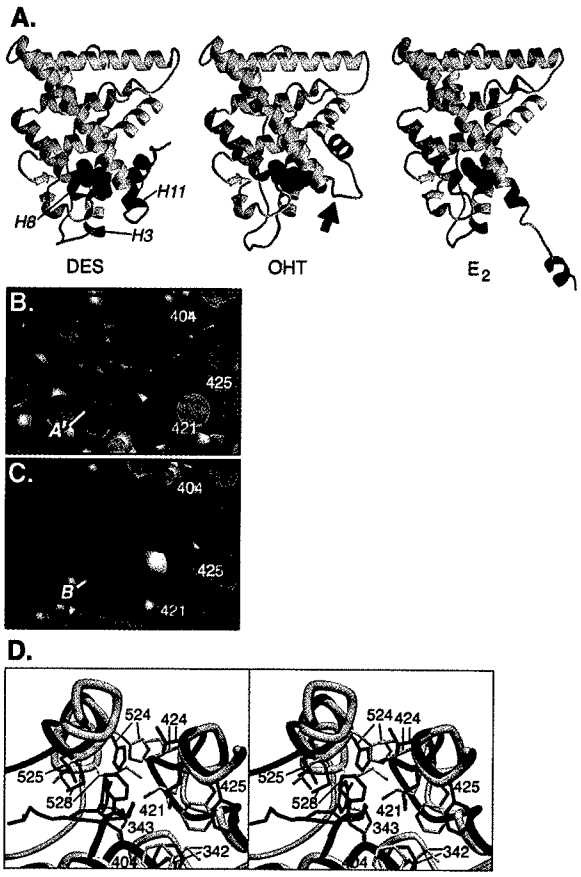

Figure 6. The Binding of Agonists and Antagonists Promote Different LBD Conformations

(A) Ribbon representations of the DES complex (without the coactivator peptide), the OHT complex, and the E_2 complex of Tanenbaum et al. (1998). The hormones are shown in space-filling representation. In each complex, helix 12 is colored magenta, and the main chain of residues 339 to 341, 421 to 423, and 527 to 530 is colored red. Helices 3, 8, and 11 (H3, H8, and H11, respectively) are labeled in the DES complex.

(B) A cross section of a space-filling model of the LBD bound to DES (green) showing the ligand completely embedded in the ligand-binding cavity. The A′ ring of DES (A′), Phe-404 (404), Met-421 (421), and Phe-425 (425) are labeled. The carbon atoms of side chain of Met-421 are colored magenta, and the sulfur atom is colored yellow.

(C) A cross section of a space-filling model of the LBD bound to OHT (red). The view is equivalent to that in (B). The B rings of OHT (B), Phe-404 (404), Met-421 (421), and Phe-425 (425) are labeled. The side chain of Met-421 is colored as in (B). The conformation of the B ring forces Met-421 to adopt a different conformation than the one it adopts in the DES complex (compare with [B]).

(D) The structures of the OHT complex and the DES complex were overlapped as in Figure 5. OHT is colored red, and DES is colored green. The A rings of both ligands point out of the page; the B ring of OHT and the A′ ring of DES point into the page. The LBD bound to OHT is colored blue, and the LBD bound to DES is colored light gray. The side chains of some of the residues whose conformations are dramatically different between the two complexes are drawn: Met-342 (342); Met-343 (343); Phe-404 (404); Met-421 (421); Ile-424 (424); Phe-425 (425); His-524 (524); Leu-525 (525); Met-528 (528). The sulfur atom of Met-421 is colored yellow in both structures.

Discussion

The AF-2 Surface and NR Box Recognition

The structure of the ERα LBD in complex with the GRIP1 NR box II peptide reveals that the LXXLL motif forms the core of a short amphipathic α helix that is recognized by a highly complementary groove on the surface of the receptor. In agreement with the conclusions of other mutational and structural studies (Brzozowski et al., 1997; Feng et al., 1998), we propose that this peptide-binding groove formed by residues from helices 3, 4, 5, and 12 and the turn between helices 3 and 4 is the AF-2 surface of ERα.

Of the eleven AF-2 residues whose side chains interact with the coactivator helix (Figure 3A), only four (Lys-362, Leu-379, Gln-375, and Glu-542) are highly conserved across the nuclear receptor family (Wurtz et al., 1996). The side chains of Gln-375 and Leu-379 are predominantly buried even in the absence of GRIP1 binding and appear to form integral parts of the architecture of the AF-2 surface. In contrast, the side chains of Lys-362 and Glu-542 are largely solvent exposed in the absence of coactivator and make both nonpolar contacts and the only direct receptor-mediated polar interactions with the coactivator helix. These two capping interaction residues are perfectly positioned at opposite ends of the AF-2 surface groove not only to stabilize the main chain conformation of the coactivator but also to function as a molecular caliper; the 15 Å distance between Lys-362 and Glu-542 is well suited to measure off the ~11 Å axial length of the short, two-turn coactivator α helix (Figure 3C). Similar receptor-mediated capping interactions have also been observed in a complex between the TRβ LBD and the NR box II peptide (Darimont et al., 1998). Mutation of either of these two capping interaction residues severely cripples coactivator binding by ERα as well as by TRβ (see Results and Henttu et al., 1997; Feng et al., 1998). Hence, the formation of helix-capping interactions may be a general feature of coactivator recognition by NRs.

The hydrophobic face of the NR box helix is formed by the side chains of the three motif leucines and the isoleucine preceding the motif (Ile-689). The functional importance of the conserved leucines in receptor binding has been demonstrated by numerous studies (Le Douarin et al., 1996; Heery et al., 1997; Torchia et al., 1997; Ding et al., 1998; Voegel et al., 1998). Structural and biochemical data in this study implicate Ile-689 as another key ERα-binding determinant. In the crystal, only the side chains of the motif leucines and Ile-689 extensively contact the LBD in both noncrystallographic symmetry-related peptides. Mutation of Ile-689 to alanine reduces the ability of the NR box II peptide to inhibit the binding of GRIP1 to ERα by ~30-fold in a competition assay (data not shown). Remarkably, the residue preceding the LXXLL motif differs for the three NR boxes of GRIP1/TIF2. The sequence variability at this position may explain the apparently different affinities of the NR boxes of TIF2 for the ERα (Voegel et al., 1998).

Helix 12 and the Regulation of AF-2 Activity

ERα AF-2 activity is blocked by antagonists such as OHT and RAL. The most striking feature of the structures of the OHT- and RAL-liganded ERα LBDs is that helix 12 is bound to the static region of the coactivator recognition groove (Figure 3B and Brzozowski et al., 1997). A comparison of these two structures with the structure of the coactivator/LBD complex reveals that in the antagonist complexes, the region of helix 12 with an NR box–like sequence (LXXML versus LXXLL) functions as an intramolecular mimic of the coactivator helix (Figure 5 and Brzozowski et al., 1997). Consistent with the proposals of others (Brzozowski et al., 1997; Darimont et al., 1998), this disposition of helix 12 directly affects the structure and function of the AF-2 surface in two ways. First, because helix 12 residues form an integral part of the AF-2 surface, the AF-2 surface is incomplete when helix 12 is in the antagonist-bound conformation. In particular, Leu-539, Glu-542, and Met-543 are incorrectly oriented for coactivator recognition. Second, residues from the static region of the AF-2 surface are bound to helix 12 and are prevented from interacting with coactivator (Figures 3A and 3B).

The sequence similarity of helix 12 of the ERα LBD to the LXXLL motif is not shared by all other NRs; the identities of the residues in this region of helix 12 in most NRs, although generally hydrophobic in character, do not as closely resemble the sequence of an NR box as those of ERα (Wurtz et al., 1996). However, it is possible that an intramolecular inhibitor with a suboptimal recognition sequence would compete for coactivator binding given its extremely high local concentration. Therefore, it will be necessary to determine if the antagonists of other NRs act by the same mechanism.

The Structural Basis of OHT Antagonism

The binding of OHT to ERα promotes a helix 12 conformation that inhibits binding of coactivator. OHT does not directly interact with any helix 12 residues (Figure 4B). Moreover, the structure of the LBD in the region of the AF-2 surface groove that interacts with helix 12 in the OHT complex is the same in the DES and E_2 complexes (Figures 3A, 3B, and 5) (Brzozowski et al., 1997). So how does OHT binding influence the position of helix 12?

Numerous studies have demonstrated the importance of the OHT side chain in receptor antagonism (Jordan and Gosden, 1982; Robertson et al., 1982). A comparison of the structures of the OHT and DES complexes reveals that the binding mode of the OHT side chain precludes the agonist-induced conformation of helix 12. The OHT side chain projects out of the ligand-binding pocket between helices 3 and 11 (Figures 2B, 6B, and 6C). As a result, the positioning of helix 12 over the ligand-binding pocket, as it is in the agonist-bound conformation, would bury the positively charged dimethylamino group of the OHT side chain within a hydrophobic cavity and produce steric clashes between the dimethylaminoethyl region of side chain and the side chain of Leu-540.

In functional terms, OHT is not, however, simply "an agonist with a side chain." OHT binding promotes a conformation of the LBD that is distinct from that stabilized by either DES or E_2 binding. These different conformations impose different restrictions on the positioning of helix 12.

Helices 3, 8, and 11 in the DES and E_2 complexes are between one to two turns longer than they are in the OHT complex (Figure 6A and Brzozowski et al., 1997). Helix 11 ends at Cys-530 in the DES and E_2 complexes and at Tyr-526 in the OHT complex. Helix 12 begins at Leu-536 in the OHT complex. This appears to be necessary; in the antagonist complex, Leu-536 forms a cooperative network of nonpolar contacts and hydrogen bonds with Glu-380 and Tyr-537 that stabilizes the N terminus of helix 12 (Figure 1B). Therefore, if helix 12 were to bind the static region of the AF-2 surface in the presence of agonist, the loop connecting helices 11 and 12 would be required to span ~17 Å over five residues. Although theoretically possible, this conformation would be highly strained and hence unlikely. In contrast, the longer loop connecting helices 11 and 12 in the OHT complex allows helix 12 to extend to the static region of the coactivator-binding groove.

In the DES and E_2 complexes, helix 12 and the loop connecting helices 11 and 12 pack against helices 3 and 11, whereas they do not in the OHT complex (Figures 2A and 2B and Brzozowski et al., 1997). Are the longer helices in the DES and E_2 complexes dependent upon the interactions helix 12 forms in the agonist-bound conformation? A recently described structure of the E_2-LBD complex suggests that they are not (Tanenbaum et al., 1998). In this structure, a crystal-packing artifact forces helix 12 to contact a symmetry-related molecule. Helix 12 is clearly not positioned over the ligand-binding pocket in this structure. Nevertheless, helices 3, 8, and 11 are longer than they are in the OHT complex (Figure 6A). Hence, the longer helices of the agonist complexes occur independently of the positioning of helix 12 over the ligand-binding pocket and are instead a direct result of agonist binding.

The secondary structure differences between the agonist complexes and the OHT complex arise from distinct arrangements of packing interactions induced by the different ligands. A cooperative network of van der Waals contacts, organized around DES or E_2, between various hydrophobic residues from helices 3, 7, 8, and 11 and the β hairpin appears to stabilize the longer helices in the agonist complexes (Figures 4A and 6D). The placement of the OHT B ring forces many of the ligand-binding pocket residues that surround it to adopt conformations that are dramatically different from those they adopt in either the DES or E_2 structures (see Results). As a result, many of the interresidue packing interactions present in the DES and E_2 structures are either absent or altered in the OHT structure (Figure 6D). These structural distortions apparently force the main chain from residues 339 to 341, 421 to 423, and 527 to 530 (which form parts of helices 3, 8, and 11, respectively, in the agonist structures) to adopt an extended conformation in the OHT structure (Figures 6A–6D).

Therefore, the binding of OHT has two distinct effects on the positioning of helix 12, each of which contributes to antagonism. Helix 12 is prevented from being positioned over the ligand-binding pocket by the OHT side chain. In addition, the alternative packing arrangement of ligand-binding pocket residues around OHT stabilizes a conformation of the LBD that permits helix 12 to reach the static region of the AF-2 surface and mimic bound coactivator.

These mechanisms do not appear to be specific to OHT. The side chain of RAL, like that of OHT, sterically hinders the agonist-bound conformation of helix 12 (Brzozowski et al., 1997). In addition, helix 11 appears to end at Met-528 in the RAL complex. This may result from the distortions in the binding pocket in the vicinity of His-524 directed by RAL binding (Brzozowski et al., 1997).

There is a great need for the improvement of existing therapies and the development of new ones for the prevention and treatment of breast cancer. While the tissue-selective antagonism of SERMs such as OHT and RAL is the result of numerous factors (Grainger and Metcalfe, 1996; Grese et al., 1997; Jordan, 1998), dissection of the mechanisms of action of these ligands requires a comprehensive understanding of how they act on the LBD and regulate its interactions with other cellular factors. Our studies have revealed, unexpectedly, that ligand-mediated structural perturbations in and around the ligand-binding pocket, and not simply side chain effects, contribute to receptor antagonism. Adjusting the balance between these two effects provides a novel strategy for the design of improved SERMs.

Experimental Procedures

Protein Expression and Purification

Human ERα LBD (residues 297–554) was expressed in BL21(DE3)-pLysS (harboring a plasmid provided by P. Sigler) as described previously (Seielstad et al., 1995). Bacterial lysates were applied to an estradiol-Sepharose column (Greene et al., 1980), and bound hERα LBD was carboxymethylated with 5 mM iodoacetic acid (Hegy et al., 1996). Protein was eluted with 3×10^{-5} M ligand in 30–100 ml of 50 mM Tris, 1 mM EDTA, 1 mM DTT, and 250 mM NaSCN (pH 8.5). The hERα LBD was further purified by ion exchange chromatography (Resource Q, Pharmacia). Protein samples were analyzed by SDS-PAGE, native PAGE, and electrospray ionization mass spectrometry.

GST-Pulldown Assays

A fusion between GST and amino acids 282–595 of hERα was constructed by subcloning the EcoRI fragment from pSG5 ERα-LBD (Lopez et al., submitted) into pGEX-3X (Pharmacia). Mutations were introduced into this construct using the QuikChange Kit (Stratagene) or by subcloning the appropriate fragments of mutant derivatives of pSG5-ER-HEGO (Tora et al., 1989; Feng et al., 1998). All constructs were verified by automated sequencing.

The wild-type and mutant GST-LBDs were expressed in BL21(DE3) cells. The total [^{3}H]E_2 binding activity in each extract was determined by saturation analysis using a controlled pore glass bead (CPG) assay (Greene et al., 1988). GST-LBD protein levels were also monitored by Western blotting with a monoclonal antibody to hERα (H222) to confirm that the mutant GST-LBDs bound E_2 with affinities comparable to the wild-type protein. Cleared extracts containing the GST-LBDs were incubated in buffer alone (50 mM Tris [pH 7.4], 150 mM NaCl, 2 mM EDTA, 1 mM DTT, 0.5% NP-40, and a protease inhibitor cocktail) or with 1 μM of either DES or OHT for 1 hr at 4°C. Extract aliquots containing 30 pmol of binding activity, based on the CPG assay, were then incubated with 10 μl glutathione-Sepharose-4B beads (Pharmacia) for 1 hr at 4°C. Beads were washed five times with 20 mM HEPES (pH 7.4), 400 mM NaCl, and 0.05% NP-40. ^{35}S-labeled GRIP1 was synthesized using the TNT Coupled Reticulocyte Lysate System (Promega) and pSG5-GRIP1 (a gift of M. Stallcup) as the template. Immobilized GST-LBDs were incubated for 2.5 hr with 2.5 μl aliquots of crude translation reaction mixture diluted in 300 μl of Tris-buffered saline (TBS). After five washes in TBS containing 0.05% NP-40, proteins were eluted by boiling the beads for 10 min in sample buffer. Bound ^{35}S-GRIP1 was visualized by fluorography following SDS-PAGE.

Crystallization and Data Collection

Crystals of the DES-hERα LBD-GRIP1 NR box II peptide complex were obtained by hanging drop vapor diffusion at 19°C–21°C. Prior to crystallization, the DES-LBD complex was incubated with a 2- to 4-fold molar excess of the GRIP1 NR box II peptide for 7–16 hr. Samples (2 μl) of this solution (4.3 mg/ml protein) were mixed with 2 μl of the reservoir buffer consisting of 25%–27% (w/v) PEG 4000, 90 mM Tris (pH 8.75–9.0), and 180 mM Na acetate and suspended over wells of the reservoir buffer. These crystals lie in the space group $P2_1$ with cell parameters a = 54.09 Å, b = 82.22 Å, c = 58.04 Å, and β = 111.34. Two molecules of the DES-LBD complex and of the coactivator peptide form the asymmetric unit. A crystal was transferred to a cryosolvent solution containing 25% (w/v) PEG 4000, 10% (w/v) ethylene glycol, 100 mM Tris (pH 8.5), 200 mM Na acetate, and 10 μM peptide and frozen in an N_2 stream at −170°C in a rayon loop. Diffraction data were measured at −170°C using the 300 mm MAR image plate at the Stanford Synchrotron Radiation Laboratory (SSRL) beamline 7-1 (λ = 1.08 Å).

Crystals of the OHT-hERα LBD complex were obtained by hanging drop vapor diffusion at 21°C–23°C. Samples (2 μl) of a solution containing 3.9 mg/ml complex and 2 μl of the reservoir solution containing 9% (w/v) PEG 8000, 6% (w/v) ethylene glycol, 50 mM HEPES (pH 6.7), and 200 mM NaCl were mixed and suspended over wells of the reservoir solution. These crystals lie in the space group $P6_522$ with cell parameters a = b = 58.24 Å and c = 277.47 Å. The asymmetric unit consists of a single LBD monomer; the dimer axis lies along a crystallographic 2-fold. A crystal was briefly incubated in a cryoprotectant solution consisting of 10% (w/v) PEG 8000, 25% (w/v) ethylene glycol, 50 mM HEPES (pH 7.0), and 200 mM NaCl and then flash frozen in liquid N_2 suspended in a rayon loop. Diffraction data were measured at −170°C at SSRL beamline 9-1 (λ = 0.98 Å) using a 345 MAR image plate.

The images of both data sets were processed with DENZO (Otwinowski and Minor, 1997), and both data sets were scaled with SCALEPACK (Otwinowski and Minor, 1997) using the default −3σ cutoff.

Structure Determination and Refinement

Our initial efforts to determine the structure of the DES-LBD-peptide complex utilized a low resolution (3.1 Å) data set (data not shown). The two LBDs in the asymmetric unit were located by molecular replacement in AMoRe (CCP4, 1994) using a partial polyalanine model of the human retinoic acid receptor γ LBD (Renaud et al., 1995) as the search probe (R= 58.2%, CC= 35.6% after placement of both monomers). Iterative cycles of 2-fold NCS averaging in DM (CCP4, 1994) interspersed with model building in MOLOC (Muller et al., 1988) and model refinement in REFMAC (Murshudov et al., 1997) (using tight NCS restraints and phases from 2-fold averaging) were used to quickly build a model of the LBD alone. For this procedure, MAMA (Kleywegt and Jones, 1994) was used for all mask manipulations, and PHASES (Furey and Swaminathan, 1990) and the CCP4 suite (CCP4, 1994) were used for the generation of structure factors and the calculation of weights.

At this point, although the DES-LBD complex model accounted for ~90% of the scattering matter in the asymmetric unit, refinement was being hampered by severe model bias. The OHT complex data set was then collected (Table 1). Starting with one of the monomers of the preliminary DES-LBD model as the search probe, molecular replacement in AMoRe was used to search for the location of LBD in this crystal form in both $P6_122$ and $P6_522$. A translation search in $P6_522$ yielded the correct solution (R= 53.8%, CC = 38.2%). In order to reduce model bias, DMMULTI (CCP4, 1994) was then used to project averaged density from the DES complex cell into the OHT complex cell. Using MOLOC, a model of the LBD was built into the resulting density. The model was refined initially in REFMAC and later with the simulated annealing, positional, and B-factor refinement protocols in X-PLOR (Brünger, 1996) using a maximum-likelihood target (Adams et al., 1997). Anisotropic scaling and a bulk solvent correction were used, and all B-factors were refined isotropically. Except for the R_{free} set (a random sampling consisting of 8% of the data set), all data between 41 and 1.9 Å (with no σ cutoff) were included. The final model consists of residues 306–551, the ligand, and 79 waters. According to PROCHECK (CCP4, 1994), 91.6% of all residues in the model are in the core regions of the Ramachandran plot and none are in the disallowed regions.

The high resolution data set of the DES-LBD NR box II peptide complex (Table 1) became available when the R_{free} of the OHT-LBD model was ~31%. Both monomers in the asymmetric unit of the DES complex crystal were relocated using AMoRe and the incompletely refined OHT-LBD model (with helix 12 and the loop between helices 11 and 12 removed) as the search model. The missing parts of the model were built, and the rest of the model was corrected using MOLOC and 2-fold averaged maps generated in DM. Initially, refinement was carried out with REFMAC, using tight NCS restraints. At later stages, the model was refined without NCS restraints using the simulated annealing, positional, and B-factor refinement protocols in X-PLOR and a maximum-likelihood target. All B-factors were refined isotropically, and anisotropic scaling and a bulk solvent correction were used. The R_{free} set contains a random sample of 6.5% of all data. In refinement, all data between 27 and 2.03 Å (with no σ cutoff) were used. The final model is composed of residues 305–549 of monomer A, residues 305–461 and 470–549 of monomer B, residues 687–697 of peptide A, residues 686–696 of peptide B, two ligand molecules, 147 waters, two carboxymethyl groups, and a chloride ion. According to PROCHECK, 93.7% of all residues in the model are in the core regions of the Ramachandran plot, and none are in the disallowed regions.

Illustrations

Figures 3C and 3D were created using GRASP (Nicholls et al., 1991). Figures 1, 2, 3A, 3B, 5, 6A, and 6D were generated using BOBSCRIPT (Esnouf, 1997) and rendered using Raster3D (Merritt and Anderson, 1994). Figure 4 was generated using LIGPLOT (Wallace et al., 1995), and Figures 6B and 6C were created using MidasPlus (Huang et al., 1991). Figure 1A depicts peptide B; all other illustrations of the coactivator peptide depict peptide A.

Acknowledgments

This work has been supported by funds from the U.S. Army Medical and Research Material Command grant DAMD 17-94-J-4228 (G. L. G.), the NCI Cancer Center Support grant P30 CA-14599 (G. L. G.), the Howard Hughes Medical Institute (D. A. A.), the NIGMS grant GM31627 (D. A. A.), the American Cancer Society grant BE61 (P. J. K.), and the NIH grant DK51083 (P. J. K.). A. K. S. was supported by a Howard Hughes Medical Institute Predoctoral Fellowship and a UCSF Chancellor's Fellowship. The Stanford Synchrotron Radiation Laboratory (SSRL) is funded by the Department of Energy, Office of Basic Energy Science. We thank H. Deacon, P. Foster, T. Mau, N. Sauter, and the staff of SSRL for assistance with data collection; C. Anderson, C. Hospelhorn, and T. McSherry for assistance with the biochemical experiments; and M. Butte, B. Darimont, R. Keenan, T. Mau, R. Wagner, and K. Yamamoto for comments on the manuscript. We would especially like to thank R. Wagner for contributions at the early stages of the project; D. Tanenbaum, Y. Wang, and P. Sigler for providing us their E_2-LBD coordinates in advance of publication; and H. Deacon and A. Derman for cheerful and extensive assistance with the figures and the manuscript, respectively.

Received September 1, 1998; revised November 16, 1998.

References

Adams, P.D., Pannu, N.S., Read, R.J., and Brünger, A.T. (1997). Cross-validated maximum likelihood enhances crystallographic simulated annealing refinement. Proc. Natl. Acad. Sci. USA *94*, 5018–5023.

Anzick, S.L., Kononen, J., Walker, R.L., Azorsa, D.O., Tanner, M.M., Guan, X.-Y., Sauter, G., Kallioniemi, O.-P., Trent, J.M., and Meltzer, P.S. (1997). AIB1, a steroid receptor coactivator amplified in breast and ovarian cancer. Science *277*, 965–968.

Beato, M., Herrlich, P., and Schutz, G. (1995). Steroid hormone receptors: many actors in search of a plot. Cell *83*, 851–857.

Berry, M., Metzger, D., and Chambon, P. (1990). Role of the two activating domains of the oestrogen receptor in the cell-type and

promoter-context dependent agonistic activity of the anti-oestrogen 4-hydroxytamoxifen. EMBO J. *9*, 2811–2818.

Bourguet, W., Ruff, M., Chambon, P., Gronemeyer, H., and Moras, D. (1995). Crystal structure of the ligand-binding domain of the human nuclear receptor RXR-α. Nature *375*, 377–382.

Brünger, A.T. (1996). X-PLOR Version 3.843 (New Haven, CT: Yale University).

Brzozowski, A., Pike, A., Dauter, Z., Hubbard, R., Bonn, T., Engstrom, O., Ohman, L., Greene, G., Gustafsson, J., and Carlquist, M. (1997). Molecular basis of agonism and antagonism in the oestrogen receptor. Nature *389*, 753–758.

CCP4. (1994). The CCP4 suite: programs for protein crystallography. Acta Crystallogr. D *50*, 760–763.

Chen, H., Lin, R.J., Schiltz, R.L., Chakravarti, D., Nash, A., Nagy, L., Privalsky, M.L., Nakatani, Y., and Evans, R.M. (1997). Nuclear receptor coactivator ACTR is a novel histone acetyltransferase and forms a multimeric activation complex with P/CAF and CBP/p300. Cell *90*, 569–580.

Danielian, P., White, R., Lees, J., and Parker, M. (1992). Identification of a conserved region required for hormone dependent transcriptional activation by steroid hormone receptors. EMBO J. *11*, 1025–1033.

Ding, S., Anderson, C., Ma, H., Hong, H., Uht, R., Kushner, P., and Stallcup, M. (1998). Nuclear receptor-binding sites of coactivators glucocorticoid receptor interacting protein 1 (GRIP1) and steroid receptor coactivator 1 (SRC-1): multiple motifs with different binding specificities. Mol. Endocrinol. *12*, 302–313.

Esnouf, R.M. (1997). An extensively modified version of MolScript that includes greatly enhanced coloring capabilities. J. Mol. Graph. Model. *15*, 132–134.

Feng, W., Ribeiro, R.C., Wagner, R.L., Nguyen, H., Apriletti, J.W., Fletterick, R.J., Baxter, J.D., Kushner, P.J., and West, B.L. (1998). Hormone-dependent coactivator binding to a hydrophobic cleft on nuclear receptors. Science *280*, 1747–1749.

Furey, W., and Swaminathan, S. (1990). PA33. Am. Cryst. Assoc. Mtg. Abstr. *18*, 73.

Glass, C.K., Rose, D.W., and Rosenfeld, M.G. (1997). Nuclear receptor coactivators. Curr. Opin. Cell Biol. *9*, 222–232.

Gradishar, W.J., and Jordan, V.C. (1997). Clinical potential of new antiestrogens. J. Clin. Oncol. *15*, 840–852.

Grainger, D.J., and Metcalfe, J.C. (1996). Tamoxifen: teaching an old drug new tricks? Nat. Med. *2*, 381–385.

Greene, G., Nolan, C., Engler, J., and Jensen, E. (1980). Monoclonal antibodies to human estrogen receptor. Proc. Natl. Acad. Sci. USA *77*, 5115–5119.

Greene, G., Harris, K., Bova, R., Kinders, R., Moore, B., and Nolan, C. (1988). Purification of T47D human progesterone receptor and immunochemical characterization with monoclonal antibodies. Mol. Endocrinol. *2*, 714–726.

Grese, T.A., Sluka, J.P., Bryant, H.U., Cullinan, G.J., Glasebrook, A.L., Jones, C.D., Matsumoto, K., Palkowitz, A.D., Sato, M., Termine, J.D., et al. (1997). Molecular determinants of tissue selectivity in estrogen receptor modulators. Proc. Natl. Acad. Sci. USA *94*, 14105–14110.

Hanstein, B., Eckner, R., DiRenzo, J., Halachmi, S., Liu, H., Searcy, B., Kurokawa, R., and Brown, M. (1996). p300 is a component of an estrogen receptor coactivator complex. Proc. Natl. Acad. Sci. USA *93*, 11540–11545.

Heery, D., Kalkhoven, E., Hoare, S., and Parker, M. (1997). A signature motif in transcriptional co-activators mediates binding to nuclear receptors. Nature *387*, 733–736.

Hegy, G., Shackleton, C., Carlquist, M., Bonn, T., Engstrom, O., Sjoholm, P., and Witkowska, H. (1996). Carboxymethylation of the human estrogen receptor ligand-binding domain-estradiol complex: HPLC/ESMS peptide mapping shows that cysteine 447 does not react with iodoacetic acid. Steroids *61*, 367–373.

Henttu, P.M., Kalkhoven, E., and Parker, M.G. (1997). AF-2 activity and recruitment of steroid receptor coactivator 1 to the estrogen receptor depend on a lysine residue conserved in nuclear receptors. Mol. Cell. Biol. *17*, 1832–1839.

Hong, H., Kohli, K., Trivedi, A., Johnson, D.L., and Stallcup, M.R. (1996). GRIP1, a novel mouse protein that serves as a transcriptional coactivator in yeast for the hormone binding domains of steroid receptors. Proc. Natl. Acad. Sci. USA *93*, 4948–4952.

Horwitz, K.B., Jackson, T.A., Bain, D.L., Richer, J.K., Takimoto, G.S., and Tung, L. (1996). Nuclear receptor coactivators and corepressors. Mol. Endocrinol. *10*, 1167–1177.

Huang, C.C., Pettersen, E.F., Klein, T.E., Ferrin, T.E., and Langridge, R. (1991). Conic: a fast renderer for space-filling molecules with shadows. J. Mol. Graph. *9*, 230–236, 242.

Jordan, V.C. (1998). Antiestrogenic action of raloxifene and tamoxifen: today and tomorrow. J. Natl. Cancer Inst. *90*, 967–971.

Jordan, V.C., and Gosden, B. (1982). Importance of the alkylaminoethoxy side-chain for the estrogenic and antiestrogenic actions of tamoxifen and trioxifene in the immature rat uterus. Mol. Cell. Endocrinol. *27*, 291–306.

Kamei, Y., Xu, L., Heinzel, T., Torchia, J., Kurokawa, R., Gloss, B., Lin, S.C., Heyman, R.A., Rose, D.W., Glass, C.K., and Rosenfeld, M.G. (1996). A CBP integrator complex mediates transcriptional activation and AP-1 inhibition by nuclear receptors. Cell *85*, 403–414.

Kato, S., Endoh, H., Masuhiro, Y., Kitamoto, T., Uchiyama, S., Sasaki, H., Masushige, S., Gotoh, Y., Nishida, E., Kawashima, H., et al. (1995). Activation of the estrogen receptor through phosphorylation by mitogen-actived protein kinase. Science *270*, 1491–1494.

Kleywegt, G.J., and Jones, T.A. (1994). Halloween...masks and bones. In From First Map to Final Model, S. Bailey, R. Hubbard, and D. Waller, eds. (Warrington, England: SERC Daresbury Laboratory).

Korach, K. (1994). Insights from the study of animals lacking functional estrogen receptor. Science *266*, 1524–1527.

Kuiper, G.G., Carlsson, B., Grandien, K., Enmark, E., Haggblad, J., Nilsson, S., and Gustafsson, J.A. (1997). Comparison of the ligand binding specificity and transcript tissue distribution of estrogen receptors alpha and beta. Endocrinology *138*, 863–870.

Kumar, V., Green, S., Stack, G., Berry, M., Jin, J.-R., and Chambon, P. (1987). Functional domains of the human estrogen receptor. Cell *51*, 941–951.

Le Douarin, B., Nielsen, A.L., Garnier, J.M., Ichinose, H., Jeanmougin, F., Losson, R., and Chambon, P. (1996). A possible involvement of TIF1 alpha and TIF1 beta in the epigenetic control of transcription by nuclear receptors. EMBO J. *15*, 6701–6715.

Li, H., Gomes, P.J., and Chen, J.D. (1997). RAC3, a steroid/nuclear receptor-associated coactivator that is related to SRC-1 and TIF2. Proc. Natl. Acad. Sci. USA *94*, 8479–8484.

Merritt, E.A., and Anderson, W.F. (1994). Raster3D Version 2.0: a program for photorealistic molecular structures. Acta Crystallogr. D *50*, 219–220.

Moras, D., and Gronemeyer, H. (1998). The nuclear receptor ligand-binding domain: structure and function. Curr. Opin. Cell Biol. *10*, 384–391.

Muller, K., Amman, H.J., Doran, D.M., Gerber, P.R., Gubernator, K., and Schrepfer, G. (1988). MOLOC: A molecular modeling program. Bull. Soc. Chim. Belg. *97*, 655–667.

Murshudov, G.N., Vagin, A.A., and Dodson, E.J. (1997). Refinement of macromolecular structures by the maximum-likelihood method. Acta Crystallogr. D *53*, 240–255.

Nicholls, A., Sharp, K., and Honig, B. (1991). Protein folding and association: insights from the interfacial and thermodynamic properties of hydrocarbons. Proteins *11*, 281–296.

Norris, J.D., Fan, D., Stallcup, M.R., and McDonnell, D.P. (1998). Enhancement of estrogen receptor transcriptional activity by the coactivator GRIP-1 highlights the role of activation function 2 in determining estrogen receptor pharmacology. J. Biol. Chem. *273*, 6679–6688.

Onate, S.A., Tsai, S.Y., Tsai, M.-J., and O'Malley, B.W. (1995). Sequence and characterization of a coactivator for the steroid hormone receptor family. Science *270*, 1354–1357.

Otwinowski, Z., and Minor, W. (1997). Processing of x-ray diffraction data collected in oscillation mode. Methods Enzymol. *276*, 307–326.

Renaud, J., Rochel, N., Ruff, M., Vivat, V., Chambon, P., Gronemeyer,

H., and Moras, D. (1995). Crystal structure of the RAR-γ ligand-binding domain bound to all-trans retinoic acid. Nature *378*, 681–689.

Robertson, D.W., Katzenellenbogen, J.A., Hayes, J.R., and Katzenellenbogen, B.S. (1982). Antiestrogen basicity—activity relationships: a comparison of the estrogen receptor binding and antiuterotrophic potencies of several analogues of (Z)-1,2-diphenyl-1-[4-[2-(dimethylamino)ethoxy]phenyl]-1- butene (tamoxifen, Nolvadex) having altered basicity. J. Med. Chem. *25*, 167–171.

Seielstad, D., Carlson, K., Katzenellenbogen, J., Kushner, P., and Greene, G. (1995). Molecular characterization by mass spectrometry of the human estrogen receptor ligand-binding domain expressed in *Escherichia coli*. Mol. Endocrinol. *9*, 647–658.

Smigel, K. (1998). Breast cancer prevention trial shows major benefit, some risk. J. Natl. Cancer Inst. *90*, 647–648.

Smith, E., Boyd, J., Frank, G., Takahashi, H., Cohen, R., Specker, B., Williams, T., Lubahn, D., and Korach, K. (1994). Estrogen resistance caused by a mutation in the estrogen-receptor gene in a man. N. Engl. J. Med. *331*, 1056–1061.

Tanenbaum, D.M., Wang, Y., Williams, S.P., and Sigler, P.B. (1998). Crystallographic comparison of the estrogen and progesterone receptor's ligand binding domains. Proc. Natl. Acad. Sci. USA *95*, 5998–6003.

Tora, L., Mullick, A., Metzger, D., Ponglikitmongkol, M., Park, I., and Chambon, P. (1989). The cloned human oestrogen receptor contains a mutation which alters its hormone binding properties. EMBO J. *8*, 1981–1986.

Torchia, J., Rose, D., Inostroza, J., Kamel, Y., Westin, S., Glass, C., and Rosenfeld, M. (1997). The transcriptional co-activator p/CIP binds CBP and mediates nuclear-receptor function. Nature *387*, 677–684.

Tsai, M.J., and O'Malley, B.W. (1994). Molecular mechanisms of action of steroid/thyroid receptor superfamily members. Annu. Rev. Biochem. *63*, 451–486.

Voegel, J.J., Heine, M.J.S., Zechel, C., Chambon, P., and Gronemeyer, H. (1996). TIF2, a 160 kDa transcriptional mediator for the ligand-dependent activation function AF-2 of nuclear receptors. EMBO J. *15*, 3667–3675.

Voegel, J.J., Heine, M.J., Tini, M., Vivat, V., Chambon, P., and Gronemeyer, H. (1998). The coactivator TIF2 contains three nuclear receptor-binding motifs and mediates transactivation through CBP binding-dependent and -independent pathways. EMBO J. *17*, 507–519.

Wallace, A.C., Laskowski, R.A., and Thornton, J.M. (1995). LIGPLOT: a program to generate schematic diagrams of protein-ligand interactions. Protein Eng. *8*, 127–134.

Wrenn, C., and Katzenellenbogen, B. (1993). Structure-function analysis of the hormone binding domain of the human estrogen receptor by region-specific mutagenesis and phenotypic screening in yeast. J. Biol. Chem. *268*, 24089–24098.

Wurtz, J.M., Bourguet, W., Renaud, J.P., Vivat, V., Chambon, P., Moras, D., and Gronemeyer, H. (1996). A canonical structure for the ligand-binding domain of nuclear receptors. Nat. Struct. Biol. *3*, 87–94.

Brookhaven Protein Data Bank Accession Numbers

Coordinates have been deposited with the PDB for the DES-ERα LBD-GRIP1 NR box II peptide complex (2ERD) and for the OHT-ERα LBD complex (2ERT).

Note Added in Proof

During the course of this work, we received a draft of a manuscript (Darimont, B.D., et al. [1998]. Structure and specificity of nuclear receptor-coactivator interactions. Genes Dev. *12*, 3343–3356) describing structural studies of the complex between TRβ and the GRIP1 NR box II peptide and biochemical studies of GRIP1 binding to TRβ and GR. We have included references to this work in the text as Darimont et al. (1998). The general features of the TRβ/GRIP1 NR box II peptide complex and the recently described PPARγ/SRC-1 peptide complex (Nolte, R.T., et al. [1998]. Ligand binding and co-activator assembly of the peroxisome proliferator-activated receptor-γ. Nature *395*, 137–143) are very similar to those of the ERα/GRIP1 NR box II peptide complex discussed here, suggesting that the mechanisms of NR box recognition are conserved across NRs.

Lessons Learned about the Action of SERMs from the 3D Structure of Human Estrogen Receptors

Geoffrey L. Greene, M.D.

Estrogens and estrogen antagonists induce characteristic conformational changes in the estrogen receptor (ERα/β) that influence dimerization, phosphorylation, interaction with general and specific effector molecules, recognition of specific DNA response elements in target genes, and modulation of transcriptional activity. Many of these processes are tissue- and promoter-specific, which can change the balance between the agonistic or antagonistic behavior of a given ligand. Tamoxifen and raloxifene represent a growing class of diverse molecules known as selective estrogen receptor modulators (SERMs), which can be distinguished from pure estrogens by their ability to act either as estrogens (agonist) or as antiestrogens (antagonist) in different tissues, gene contexts and hormone environments.

To better understand this selective behavior, the structures of the human ERα ligand binding domain (ERα-LBD) complexed with several estrogen agonists and antagonists were determined. Insight into the molecular basis of estrogen agonism and antagonism was revealed by the crystal structure of the human ERα ligand binding domain (LBD) complexed with estradiol and raloxifene. Key differences in the positioning and presentation of certain regions in the hormone binding domain can explain at least some of the observed biological differences associated with estrogens and antiestrogens. Although agonist and antagonist bind at the same site within the core of the LBD, each induces a distinct conformation in the transactivation domain (AF-2) of the LBD, especially in the positioning of helix 12, providing the first structural evidence of a mechanism for selective antagonism in the nuclear receptor family. Because different estrogen antagonists vary in their ability to inhibit estrogen action in certain tissues, like the uterus, we have also focused on determining the structure of ERα LBD bound to other biologically distinct estrogens and antiestrogens. The structure of ERα LBD bound to 4-hydroxytamoxifen (OHT), the active metabolite of tamoxifen, was recently solved. In addition, we have determined the structure of ERα LBD as a complex with diethylstilbestrol (DES), a powerful synthetic estrogen, and a peptide derived from an essential interaction motif found in several related nuclear receptor transcriptional coactivators that are required for estrogen action. Interestingly, the OHT and DES structures collectively reveal and define a multipurpose cleft, or docking site, on Erα.

In addition, a comparison of the two structures reveals that there are two distinct mechanisms by which structural features of OHT promote an "autoinhibitory" helix 12 conformation in the ERα LBD. Helix 12 positioning is determined both by steric considerations, such as the presence of an extended side chain in the ligand, and by local structural distortions in and around the ligand binding pocket. Thus, one would predict that effective estrogen antagonists do not require bulky or extended side chains, which is known to be the case. In addition, the recently published structure for ERα bound to genistein, a partial agonist and environmental estrogen, demonstrates that helix 12 may assume at least one additional conformation, suggesting that the positioning of H12 may be more dynamic than assumed from previous structure determinations.

It is anticipated that ERα/β structure information will ultimately help explain how mixed estrogens/antiestrogens, like tamoxifen and raloxifene, are able to elicit selective biological effects, via one or both receptors, in different tissues. In addition, with the design and/or natural occurrence of compounds that selectively target ERα or ERβ, structure information should help reveal the molecular basis for such behavior. The data thus obtained will have an impact both on our understanding SERMs as well as on the design and use of such compounds for the treatment and prevention of breast and uterine cancers while maintaining beneficial estrogenic effects on bone, vasculature, and brain.

References

Brzozowski AM, Pike ACW, Dauter Z, et al. Molecular basis of agonism and antagonism in the oestrogen receptor. Nature, 389, 753-758 (1997).

Shiau AK, Barstad D, Loria PM , et al. The structural basis of estrogen receptor/coactivator recognition and the antagonism of this interaction by tamoxifen. Cell, 95, 927-937 (1998).

Advances in Human Breast and Prostate Cancer, Keystone Symposia on Molecular and Cellular Biology, March 19-24, 2000, Incline Village, Nevada.

Structure-Function Studies of Human Estrogen Receptors: Therapeutic Strategies

Geoffrey Greene,[+] Andrew Shiau,[*] Danielle Barstad[+] and David Agard[*] .[+]Ben May Institute for Cancer Research, University of Chicago, Chicago, Illinois 60637; [*]Howard Hughes Medical Institute and the Department of Biochemistry & Biophysics, University of California at San Francisco.

Insight into the molecular basis of estrogen agonism and antagonism has been revealed by the crystal structures of the human ERα ligand binding domain (LBD) complexed with estradiol, raloxifene, 4-hydroxytamoxifen (OHT) and diethylstilbestrol (DES) plus a peptide derived from an essential interaction motif found in several related nuclear receptor transcriptional coactivators. Although agonists and antagonists bind at the same site within the core of the LBD, each induces distinct conformations in the transactivation domain (AF-2) of the LBD, especially in the positioning of helix 12, providing structural evidence of a mechanism for selective antagonism in the nuclear receptor family. Interestingly, the OHT and DES structures collectively reveal and define a multipurpose docking site on ERα that can accommodate either helix 12 or one of several coregulators. In addition, a comparison of the two structures reveals that there are two distinct mechanisms by which structural features of OHT promote an "autoinhibitory" helix 12 conformation. Helix 12 positioning is determined both by steric considerations, such as the presence of an extended side chain in the ligand, and by local structural distortions in and around the ligand binding pocket. Thus, one would predict that effective estrogen antagonists do not necessarily require bulky or extended side chains. It is anticipated that ERα/β structure information will ultimately help explain how mixed estrogens/antiestrogens, like tamoxifen and raloxifene, are able to elicit selective biological effects, via one or both known ERs, in different tissues. In addition, with the design and/or natural occurrence of compounds that selectively target ERα or ERβ, structure information should help reveal the molecular basis for such behavior.

Eurocancer 2000, June 5-7, 2000, Paris, France.

Structure analyses of SERM complexes with estrogen receptors: implications for drug design

Geoffrey L. Greene, The Ben May Institute for Cancer Research, The University of Chicago, Chicago, Illinois, USA.

Estrogens and estrogen antagonists induce characteristic conformational changes in the two known estrogen receptors (ERα and ERβ) that influence interaction with general and specific effector molecules, recognition of specific DNA response elements in target genes, and modulation of transcriptional activity in hormone sensitive tissues and cancers. Many of these processes are tissue- and promoter-specific, which can change the balance between the agonistic or antagonistic behavior of a given ligand. Tamoxifen and raloxifene represent a growing class of diverse molecules known as selective estrogen receptor modulators (SERMs), which can be distinguished from pure estrogens by their ability to act either as estrogens (agonist) or as antiestrogens (antagonist) in different tissues, gene contexts and hormone environments. To better understand this selective behavior, the 3D structures of the human ERα ligand binding domain (ERα-LBD) complexed with several estrogen agonists and antagonists were determined.

Insight into the molecular basis of estrogen agonism and antagonism has been revealed by the crystal structures of ERα and ERβ ligand binding domains (LBDs) complexed with several ligands, including estradiol (E2) (1), diethylstilbestrol (DES) (2), raloxifene (RAL) (1), 4-hydroxy-tamoxifen (OHT) (2), and genistein (GEN) (3). For agonists like DES, inclusion of a peptide derived from an essential LXXLL interaction motif (NR box) found in several related p160 nuclear receptor transcriptional co-activators has helped define the AF-2/co-activator interface (4). Although agonists and antagonists bind at the same site within the core of the LBD, each induces distinct conformations in the transactivation domain (AF-2) of the LBD, especially in the positioning of helix 12, providing structural evidence for multiple mechanisms of selective antagonism in the nuclear receptor family. Interestingly, the OHT/RAL and DES/E2 structures collectively reveal and define a multipurpose docking site on ERα that can accommodate either helix 12 or one of several coregulators. In addition, a comparison of the two structures reveals that there are at least two distinct mechanisms by which structural features of OHT promote an "autoinhibitory" helix 12 conformation. Helix 12 positioning can be

determined both by steric considerations, such as the presence of an extended side chain in the ligand, and by local structural distortions in and around the ligand binding pocket. Thus, one would predict that effective estrogen antagonists do not necessarily require bulky or extended side chains. The recent determination of the crystallographic structures of ERα and ERβ LBDs complexed with *cis*-R, R-diethyl-tetrahydrochrysene (R,R-THC), which is an ERα agonist and an ERβ antagonist (5), provides support for this prediction.

It is anticipated that the utilization of ER subtype-specific interactions in ligand design will allow the creation of new compounds that act differently via the two ERs and possess novel therapeutic properties. In addition, with the design and/or natural occurrence of compounds that selectively target ERα or ERβ, structure information should help reveal the molecular basis for such behavior.

Citations

1. Brzozowski A, Pike A, Dauter Z, Hubbard R, Bonn T, Engstrom O, Ohman L, Greene G, Gustafsson J, Carlquist M 1997 Molecular basis of agonism and antagonism in the oestrogen receptor. Nature 389:753-758
2. Shiau AK, Barstad D, Loria PM, Cheng L, Kushner PJ, Agard DA, Greene GL 1998 The structural basis of estrogen receptor/coactivator recognition and the antagonism of this interaction by tamoxifen. Cell 95:927-37
3. Pike AC, Brzozowski AM, Hubbard RE, Bonn T, Thorsell AG, Engstrom O, Ljunggren J, Gustafsson JA, Carlquist M 1999 Structure of the ligand-binding domain of oestrogen receptor beta in the presence of a partial agonist and a full antagonist. Embo J 18:4608-18
4. Ding S, Anderson C, Ma H, Hong H, Uht R, Kushner P, Stallcup M 1998 Nuclear receptor-binding sites of coactivators glucocorticoid receptor interacting protein 1 (GRIP1) and steroid receptor coactivator 1 (SRC-1): Multiple motifs with different binding specificities. Mol Endocrinol 12:302-313
5. Meyers MJ, Sun J, Carlson KE, Katzenellenbogen BS, Katzenellenbogen JA 1999 Estrogen receptor subtype-selective ligands: asymmetric synthesis and biological evaluation of cis- and trans-5,11-dialkyl- 5,6,11, 12-tetrahydrochrysenes. J Med Chem 42:2456-68